Molecular & mechanical manipulation of membrane domains in planar supported bilayers

A Thesis
SUBMITTED TO THE FACULTY OF
UNIVERSITY OF MINNESOTA
BY

Rochelle M. Warner

IN PARTIAL FULFILLMENT OF THE REQUIREMENTS
FOR THE DEGREE OF
MASTER OF SCIENCE

Dr. Erin D. Sheets

August 2015

Acknowledgements

I would like to express my sincerest gratitude to my advisor and mentor, Dr. Erin Sheets. She has given me insurmountable guidance and encouragement in pursuing my passion for the field of science. I would also like to thank Dr. Ahmed Heikal for his unwavering enthusiasm for exploration in the pursuit of knowledge and learning. I would like to acknowledge my colleague, Tyler Floden, for not only all his time and efforts in aligning and optimizing the optical trap, but also for being an infinitely supportive friend. I would like to also thank my labmate and friend, Megan Currie, for making my experience in lab full of fun, laughs, and adventure. I would like to thank my committee for their unprecedented patience and support. I would also like to extend a sincere thank you to Spencer Gardeen for being encouraging and optimistic during the writing process. Lastly, I would like to express my deepest gratitude to my parents for believing in me throughout all my endeavors. Their love and support has made everything possible.

Abstract

Biomembranes are dynamic, two-dimensional fluids that actively participate in biological functions such as signaling, membrane trafficking, endocytosis and exocytosis. They are composed of thousands of lipid species and hundreds of proteins in cells, and the membrane itself is constantly remodeling. Nano-membrane domains are hypothesized to play an integral role in many cell signaling pathways. Their transient nature and biocomplexity underlies a myriad of fundamental questions about lipid-lipid and lipid-protein interactions and their roles in cellular functions. As a result, there is a need for innovative approaches for understanding different biophysical aspects of membrane assemblies and their underlying, multiscale dynamics.

Membranes in living cells are very complex and highly dynamic making it difficult to manipulate crosslinking at the molecular level. We overcome this issue by using light (optical trapping) to crosslink proto-domains in a well-controlled, yet non-invasive manner and quantitative fluorescence microscopy to follow the subsequent dynamics. To simplify the investigations of specific molecular interactions and their dynamics, we use biomimetic, or model, membranes that are chemically well-defined; that is, they are composed of only a few molecular species. The goal is to integrate dynamic holographic optical trapping and fluorescence imaging with fluorescence correl–ation spectroscopy to characterize membrane domain nucleation in biomimetic planar supported bilayers. Our hypothesis is that by trapping multiple microsphere-bound receptors, the associated heterogeneous lipid domains will nucleate a larger domain upon interaction in a manner that depends on the lipid type, cholesterol and protein content.

Table of Contents

List of Tables

List of Figures

List of Abbreviations

BS	beam splitter
BSA	bovine serum albumin
CCD	charged coupled device
CTxB	cholera toxin B subunit
diI-C_{18}	1,1'-dioctadecyl-3,3,3',3'-tetramethylindotricarbocyanine iodide
EDC	1-ethyl-3-(3-dimethylaminopropyl)carbodiimide HCl
FCS	fluorescence correlation spectroscopy
GM1	ganglioside GM1
HEPES	4-(2-hydroxyethyl)-1-piperazineethanesulfonic acid
HOT	holographic optical trapping
IgE	immunoglobulin E
IR	infrared
L_α	liquid-crystalline
LC	lens
L_d	liquid-disordered
LE	lens expander
L_o	liquid-ordered
MES	2-(N-morpholino)ethanesulfonic acid
NA	numerical aperture
NBD-PC	1-oleoyl-3-(12-[(7-nitro-2-1,3-benzooxadiazol-4-yl)-amino]dodecanoyl)-*sn*-glycero-3-phosphocholine
NBD-PE	1,2-dipalmitoryl-*sn*-glycero-3-phosphoethanolamine-N-(7-nitro-2-1,3-benzoxadiazol-4-yl)
PBS	phosphate-buffered saline
PC	personal computer
PMT	photomultiplier tube
POPC	1-palmitoyl-2-oleoyl-*sn*-glycero-3-phosphocholine
SLM	spatial light modulator
SM	sphingomyelin (egg, chicken)
S_o	solid state
SPT	single particle tracking
Sulfo-NHS	N-hydroxysulfosuccinimide
SUV	small unilamellar vesicle
VALAP	Vaseline:lanolin:paraffin [1:2:2 (w/w)]

List of Symbols

χ^2	chi squared
a	radius of a spherical particle
η	solvent viscosity
K	inverse of Debye-Hückel length
λ	wavelength of light
σ	scattering cross-section
τ_D	diffusion time
τ_z	diffusion along z-axis
τ_{xy}	diffusion in the plane
ω_z	axial $1/e^2$-radius
ω	structural geometric factor
ω_{xy}	lateral $1/e^2$-radius
ω_0	structural parameter
D	lateral diffusion coefficient
f	fraction
F(t)	fluorescence intensity
$F_{gradient}$	force gradient
$F_{scattering}$	scattering force
$G(\tau)$	autocorrelation function
I(x,y,z)	intensity of light
I_0	maximum intensity of light
κ_B	Boltzmann constant
l	ratio of refractive indices
N	average number of fluorescent molecules in detection volume
n	number of trials
n_i	refractive indices
n_m	refractive indices of surrounding medium
$Q_{gradient}$	efficiency of gradient optical force
Q	efficiency of trap
$Q_{scattering}$	efficiency of scattering optical force
R_h	hydrodynamic radius
R_0	particle radius
r	thickness of membranes
T	temperature
τ	lag time
t	time
W	power of laser beam
x	displacement

I: Introduction

1.1 Overview

The fluid mosaic model proposed by Singer and Nicolson created a framework to explore the significance of membranes (*1*). The importance of understanding dynamic processes, such as diffusion within biological membranes, has evolved this proposed model and given rise to its undeniable cellular complexity. The intricate composition and elaborate dynamic capabilities of membranes creates impediments in studying underlying mechanisms *in vivo*, therefore biomimetic membranes are used to control the complexity and composition of our model system.

1.2 Role of biological membranes

In its simplest form, the biological membrane creates a compartmentalized environment to maintain cellular functionality. This dynamic two-dimensional fluid regulates the exchange between a cell's interior and exterior environment through a semi-permeable membrane, allowing for biological function. These functions include transport, trafficking, cellular communication, adhesion, signal propagation, endocytosis and exocytosis (*2, 3*). The enzymatic machinery necessary for metabolic and signaling activity also resides within the membrane (*3*). Its heterogeneous composition of various lipid and protein species gives rise to the multifunctionality of biomembranes. The lipid-protein distribution across the surface actively influences membrane fluidity, dynamics and structure (*4*). These dynamic interactions create the underlying framework for

membrane structural models, which ultimately lead to the biological significance necessary for cell functionality.

The immune system has been used as a model for studying the relationship between membrane structure and functionality (*5*). In particular, it has been hypothesized that specialized cholesterol-rich membrane domains facilitate the first biochemical step in the allergic response (*6*). The first step in the allergic immune response is the crosslinking of IgE-FcεRI complexes within the plasma membranes of mast cells and basophils by multivalent antigen. As shown in Figure 1.1, this crosslinking event in turn leads to the phosphorylation of specific tyrosine residues in the cytoplasmic segments of the β and γ subunits of FcεRI by the Src family tyrosine kinase Lyn, which is anchored to the inner leaflet of the plasma membrane via N-terminal myristoylation and palmitoylation (*7, 8*). Another tyrosine kinase, Syk, is then transiently recruited to the phosphorylated IgE receptor where it too becomes tyrosine phosphorylated and activated. Syk then initiates multiple signaling cascades which lead to phospholipase C activation, calcium mobilization and, ultimately, degranulation (the exocytotic release of histamine and other inflammatory mediators) (see Figures 1.1 and 4.1). The initial phosphorylation of FcεRI by Lyn occurs in a cholesterol-dependent manner that has been hypothesized to be facilitated by cholesterol-rich membrane domains (*9*). However, these cholesterol-enriched domains have not been observed *in vivo* without substantial perturbation (e.g., long term incubation in the cold or extensive crosslinking of domain markers) (*10, 11*). New approaches to identify and follow the molecular interactions within rafts as they form and dissipate are critically needed to understand how membrane structure influences

IgE receptor signaling. The T cell antigen receptor (*12*) and B cell antigen receptor (*13*) also use cholesterol-rich lipid domains in their signal initiation, analogous to FcεRI, their sister immunoreceptor (*14-16*). Therefore, we use IgE receptor signaling as a model for investigating membrane domain participation in other signaling pathways, such as immunoreceptor and growth factor receptor (*17*) signaling. We have been investigating this signaling pathway and its functionally important molecular interactions using a variety of cell biological, biochemical and biophysical approaches. The work described in this Thesis focuses upon efforts to understand the membrane organization (that is, cholesterol-rich microdomains) using simpler model membranes as compared with those in live cells.

The primary focus of this Thesis is overcoming obstacles created by the limitations of conventional fluorescence microscopy and spectroscopy techniques by expanding traditional approaches through a multimodal system. To this end, two parallel paths have been pursued: preparing planar supported bilayers that contain the ganglioside GM1 and covalently conjugating microspheres with cholera toxin B (CTxB), which specifically binds to membrane-incorporated GM1. The CTxB-microsphere acts as a "handle" for the optical trap as will be described in Chapter 4. Fluorescence imaging is used to visualize membrane integrity, and subsequent lateral diffusion of lipid species is measured with fluorescence correlation spectroscopy (FCS). These results will ultimately lead to new insights into domain formation in membranes.

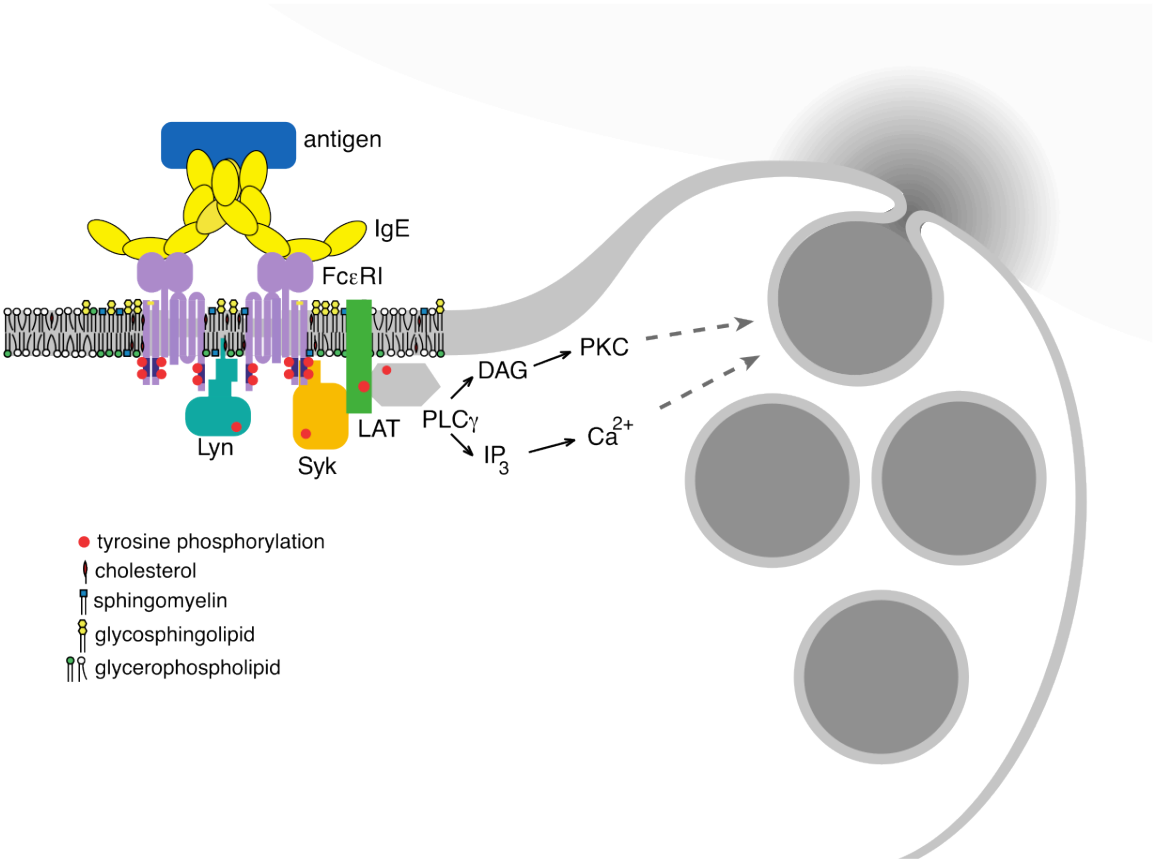

Figure 1.1 Schematic of IgE-IgE crosslinking FcεRI receptor to initiate a signaling cascade that ultimately leads to histamine release in the allergic response in mast cells.

1.3 Compositional influence on membrane structure

In 1972, Singer and Nicolson described the organization of biomembranes as a dynamic, fluid, heterogeneous sheet of lipids and proteins (*1, 18*). The fluid mosaic model has been used to describe the influence of the extracellular matrix and cytoskeleton role on creating a potential influence on membrane mobility (*4*). Thousands of lipid and hundreds of protein species in biological membranes give rise to this structural configuration. The lipid species that constitute a biomembrane are primarily phospholipids and cholesterol (*19*). Of the lipid species, phospholipids predominate and create the spontaneous, structural bilayer for membranes due to their amphipathic characteristics (*2, 3*). Phospholipids contain polar headgroups and non-polar hydrophobic tails (*3*). These headgroups vary in their size and charge (anionic, cationic, zwitterionic), while the acyl chains vary in length and saturation. Together these two components of a phospholipid affect the resulting molecular shape and intermolecular interactions to profoundly influence the physicochemical characteristics of the bilayer. The entropically driven hydrophobic interactions between lipid species excludes water to drive the formation and stability of the membrane (*4*). The hydrophilic, charged head groups interact with each other, neighboring membrane molecules, the surrounding water, and other species in the bulk solution and orient themselves to protect the hydrophobic inner leaflet consisting of acyl chains. Van der Waals and hydrophobic effects drive this orientation. The scaffold created by thermodynamically driven lipid self-organization allows for the attachment and integration of various proteins that further influence the assembly.

Sphingomyelin (SM) and phosphatidylcholine (PC) comprise over 50% of lipid species in the plasma membrane (*4*). The acyl chains can be ordered therefore comprised of long saturated tails, such as SM. Disordered hydrocarbon tails composed of unsaturated acyl characteristics, are lipid species such as PC (*19*). The chain structure influences six nearest neighbor interactions (*20*). In addition to chain order impacting lateral reorganization, the cholesterol content also affects the redistribution. Cholesterol contains a small hydroxyl headgroup allowing for it to position itself between lipid species, creating tight packing (*21, 22*). The fused ring system of cholesterol also confers rigidity to the acyl chains of neighboring lipids. An energy penalty is associated with hydrophobic mismatch and therefore the exclusion of cholesterol in particular regions of the membrane (*4*). Hydrophobic mismatch refers to any difference between length of hydrophobic portions of lipid or integral protein species within the thickness of the membrane.

Lipids undergo both lateral and rotational diffusion. Flip flop between inner and outer leaflets of the bilayer occurs at a very restricted rate and is often enzymatically driven *in vivo* (*4*). The asymmetric structure of the membrane is largely influenced by composition and influences biological processes beyond that of those dependent upon structural curvature. The asymmetric nature of the membrane creates a platform to induce cell activation and phagocytosis (*4*). The inner leaflet is enriched in amine- and serine-containing phospholipid species (*4*). The outer leaflet contains higher levels of choline-containing lipids, such as PC and SM, and therefore more prevalent levels of cholesterol due to their preferential association (*4*). Cell asymmetry not only increases

specific association with cholesterol, but also plays a critical role in the association with proteins and enzymatic activity necessary for the outer leaflet (*4*). The fluid mosaic model emphasized the fluid heterogeneity of biological membranes, but failed to explain the redistribution of membrane components in the formation of lipid domains (*4, 6, 23*).

1.4 Domains: Link between structure and function

In biological or more complex biomimetic membranes, further lateral organization with the bilayer can result. Two distinct phase assemblies containing diverse properties can distinguish this organization. The gel (solid, S_o) state can be induced by lowering the temperature below a lipid's melting temperature and is notable due to its tight packing conditions through strong hydrophobic interactions, where subsequent restricted mobility is characterized (*24*). The alternative, fluid (liquid crystalline, L_α) state is found by increasing the temperature above a lipid's melting temperature thereby creating a more dynamic condition of lateral mobility. Both phases can exist in biomimetic systems. Length and degree of saturation of hydrocarbon chains influence the assemblies. Long, saturated hydrocarbon chains are characteristic of lipids found in the S_o phase. Short, unsaturated hydrocarbon chains are characteristic of lipids found in the L_α state. The L_α phase can be further separated into liquid-ordered (L_o) or liquid-disordered (L_d) regions (Fig. 1.2). The L_o occurs due to a decrease in van der Waals interactions influenced by the association of cholesterol with lipids commonly found in the S_o assemblies creating a more ordered structure than that found in the L_d assemblies, yet more dynamic mobility than that of S_o assemblies (*4, 25, 26*). The

creation of non-uniform, non-random cooperative interactions driven by thermodynamics of membrane components possesses a key functional role (*4*). Small regions of L_o assemblies are found in the plasma membrane and are hypothesized to be platforms for signal transduction to occur (*4, 27*). L_o regions induced by the peripheral lipid species interacting and exchanging with the bulk lipid species are critical to cellular function (*4*). Domain formation or lipid de-mixing assemblies are driven by lipid and protein interactions to eliminate the energetically unfavorable hydrophobic mismatch (*4*). Several forces drive this transient process of domain formation: hydrogen bonding, electrostatic interactions, hydrophobic interactions, and van der Waals interactions (*4*). The roles of lipid-lipid, lipid-protein, and protein-protein interactions on domain formation within the bilayer is actively being investigated (*4*).

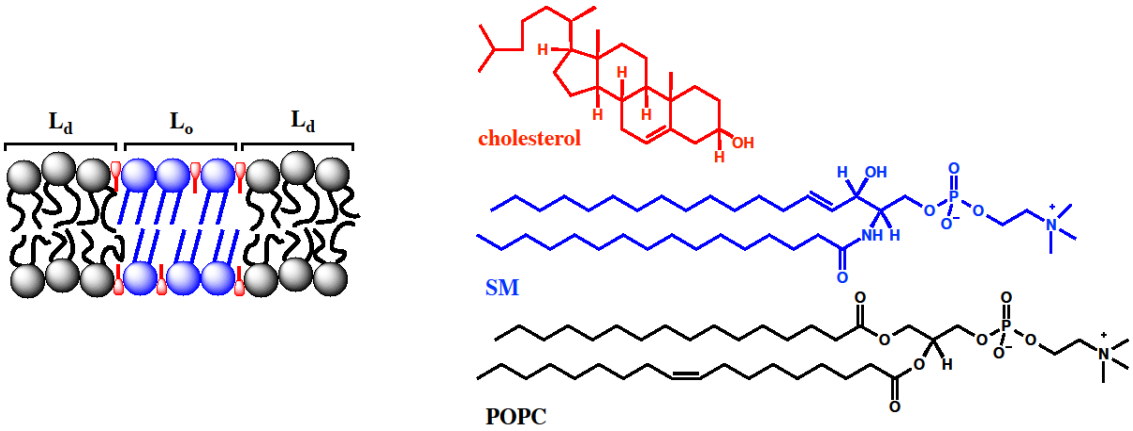

Figure 1.2 Schematic diagram of model membrane phase behavior. Liquid-ordered (L_o) regions contain cholesterol and saturated lipid species, such as sphingomyelin (SM). Liquid-disordered (L_d) regions contain unsaturated lipid species, such as 1-palmitoyl-2-oleoyl-sn-glycero-3-phosphocholine (POPC).

1.5 Biomimetic membranes

Biological membranes are inherently complex. To simplify investigation, we use biomimetic membranes that are chemically well-defined. These model systems typically contain one to three lipids and may (or may not) contain proteins. Each system has its particular pros and cons, which make it amenable to specific types of experiments. I describe some of the major model membrane systems here and end with the system that is the focus of the work described in this Thesis, that is, supported planar membranes.

Many model membrane systems are vesicular in nature, and these systems can encapsulate an aqueous component. Giant unilamellar vesicles are cell-sized, ~tens of microns in diameter, which minimize potential surface effects and curvature issues. This system has been used for phase diagram mapping (*28*) and partitioning studies (*29*), for example. Large unilamellar vesicles range in size from ~100 nm–10 μm in diameter. These are frequently used for calorimetry and binding studies (*30-33*). Small unilamellar vesicles (SUVs) have diameters < 100 nm. These vesicles have high curvatures and awkward packing between the two leaflets, which make these systems thermodynamically unstable and useful for forming supported planar bilayers.

Supported planar bilayers are amenable for imaging with a variety of techniques such as atomic force microscopy (*34, 35*), electron microscopy (*36, 37*), imaging ellipsometry (*38, 39*), and fluorescence microscopy (*3, 40-50*). The simplest means of preparing supported planar bilayers is to prepare symmetric bilayers using SUV rupture on to a clean surface such as a glass slide or electron microscopy grid (*51, 52*). A 0.5–1.5 nm layer of water between the lower leaflet and the glass substrate allows lipids to be

freely mobile within the bilayer (*53*). The work described in Chapters 3 and 4 takes advantage of this approach. Asymmetric bilayers can be prepared using Langmuir-Schaefer deposition using a Langmuir trough, or through a combination of Langmuir deposition and SUV rupture (*46, 54*). In future work, asymmetric bilayers will be prepared to extend the work described in Chapters 3 and 4.

1.6 Molecular & mechanical manipulation

A molecular and mechanical approach is used in this Thesis to overcome the many limitations of understanding the underlying mechanism of domain formation. Our model system uses fluorescent microspheres as a handle for an optical trap to manipulate their location in the *xy* plane. These microspheres are covalently coupled to cholera toxin B (CTxB) (Fig. 1.3). The mechanical manipulation of CTxB-microspheres is achieved by using infrared light as a ligand to crosslink multiple CTxB-microspheres with the potential of nucleating a domain. Chapter 2 describes the materials and methods used in these studies and includes information about optical trapping and the influence of incorporating a holographic component and the molecular approach to covalently coupling the fluorescent handle to a protein that interacts with a domain marker. The ability to induce domain nucleation and study the subsequent dynamics provides a multimodal approach to study the fundamental mechanisms that lead to biological function in membranes.

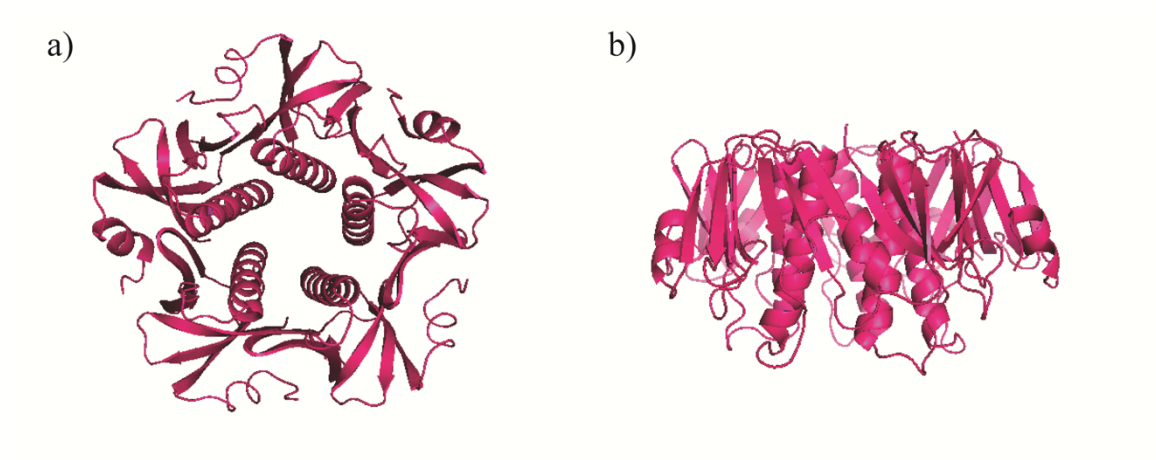

Figure 1.3 Cholera toxin B subunit structure (CTxB). Top-down view and b) side view structure of CTxB subunit pentamer [57 kDa] that binds with high affinity [$K_d < 10^{-9}$ M *in vitro (55)*] in each of its five domains to GM1 (PDB 1MD2).

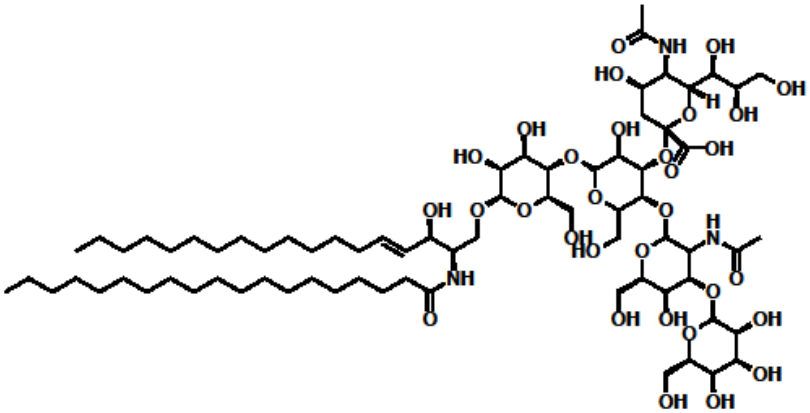

Figure 1.4 Structure of the ganglioside GM1.

In Chapter 3, I describe our efforts to characterize the lateral mobility of a ganglioside GM1 (Fig. 1.4) as a function of GM1 concentration in the planar bilayer. Interestingly, GM1 incorporation was not observed to significantly affect the lateral mobility of lipid species in planar supported bilayers. In Chapter 4, I describe our efforts to induce nucleation of cholesterol-rich nanodomains using light as our "ligand". For both projects, I exploit fluorescence imaging to assess membrane integrity and measure lipid dynamics using fluorescence correlation spectroscopy (FCS). The nucleation project introduces a novel means of optical trapping, holographic optical trapping.

II: Materials and methods

2.1 Overview

This Chapter describes the background theory of our multimodal optical system used to mechanically manipulate and quantify molecular dynamics of model membranes. The integration of these techniques on a single platform allows for measuring the lateral diffusion of lipid analogs incorporated into the membrane while spatially manipulating the position of CTxB-microspheres to generate potential domain regions. The biochemical and biophysical sample preparations and subsequent measurements are also described.

2.2 Materials and methods of model system

2.2.1 Planar supported bilayer preparation

The day prior to an FCS experiment, small unilamellar vesicles (SUVs) were prepared. Chloroform solutions of lipids (All lipids are purchased from Avanti Polar Lipids) at a desired composition (e.g., 0.1 mol% 1-oleoyl-2-(12-(7-nitro-2-1,3-benzoxadiazol-4-yl)amino]dodecanoyl-*sn*-glycero-3-phosphocholine (NBD-PC), 1-palmitoyl-2-oleoyl-*sn*-glycero-3-phosphocholine (POPC), varying ganglioside GM1 varying concentration (0, 0.05, 0.1, 0.5, 1.0 mol%) in a final 2 mM final lipid composition. The lipids were used without additional purification. Samples were placed in ethanolic KOH cleaned test tube, dried under nitrogen, resuspended in nanopure water, probe sonicated until clarified, and subjected to ultracentrifugation (Airfuge, 30 psi, 1 h). The top quarter of supernatant was collected and stored in the dark at room temperature.

On the day of the experiment, 70 μL aliquots of lipid suspensions were placed between detergent-cleaned 22 mm × 22 mm glass coverslip and 3-inch × 1-inch slide sandwiches immediately after argon plasma cleaning. They were placed in a humidified chamber for 1 h to allow the spontaneous fusion of SUVs to form a uniform bilayer. Unfused vesicles were rinsed exhaustively with nanopure water. 10 mg/mL BSA in PBS (10 mM potassium phosphate, 150 mM sodium chloride, pH 7.4) blocking agent was added to each slide and incubated in a humidified chamber for 1 h. Sandwiches were rinsed exhaustively with PBS. For some experiments, 0.1 mg/mL of covalently coupled CTxB-microsphere (Section 2.2.2 for coupling procedure) was added to each slide and incubated in humidified chamber for 30 min. A final rinse with PBS was used to removed unbound microspheres and sealed with VALAP (Vasoline:lanolin:paraffin [1:2:2, w/w]). (Note, for all experiments nanopure water (≥ 18.2 MΩ-cm) was used.)

Measurements were carried out immediately after sealing. Acquisition of lateral diffusion of lipid analog, 1-oleoyl-3-12-[(7-nitro-2-1,3-benzooxadiazol-4-yl)-amino]-dodecanoyl-sn-glycero-3-phosphocholine (NBD-PC), containing bilayers occurred with a 525/30 HQ excitation filter, 483 nm laser, 20 scans for 10 s acquisition, 50 μm optical fiber diameter with 25% use of a 50% core laser power intensity (1.05 optical density) at room temperature (Fig. 2.9). All other optical components were as described in Section 2.3.

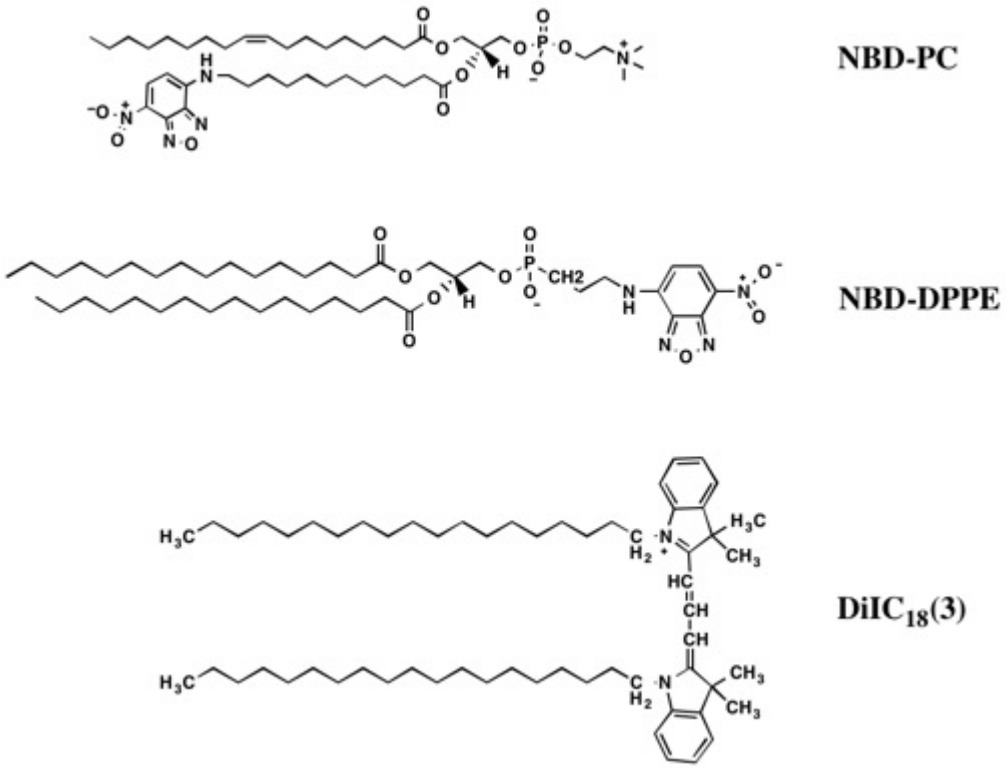

Figure 2.1 Lipid analogs incorporated into planar supported bilayers used in experimental studies described in this Thesis to measure lateral diffusion.

2.2.2 Covalently coupling of carboxylate microspheres to cholera toxin B

10 mg/mL Dragon Green uniform dyed microspheres (0.97 µm, Bangs Laboratories) were washed with 1 mL activation buffer (0.098M 2-[N-morpholino]-ethanesulfonic acid [MES, Sigma] in H_2O, pH 6.10) via centrifugation (5 min, high speed) at room temperature (*56, 57*) (Fig. 2.2). The pellet was resuspended in 1 mL of activation buffer. Under constant mixing, 19 mg of 1-ethyl-3-(3-dimethylaminopropyl) carbodiimide HCl (EDC) and 1.09 mg of N-hydroxysulfosuccinimide (Sulfo-NHS) was added. The reaction was allowed to proceed with gentle mixing at room temperature for 15 min. The pellet was washed and resuspended in 1 mL coupling buffer (1 M 4-(2-hydroxyethyl)piperazine-1-ethanesulfonic acid [HEPES], pH 7.4) under the previously mentioned washing conditions. A 1:10 (AlexaFluor 488 CTxB:CTxB) protein composition (cholera toxin B [Sigma Aldrich], recombinant [Invitrogen]) was added based on saturation of microsphere surface. The reaction was carried out for 4 h under constant mixing at room temperature. The pellet was washed and resuspended in quenching buffer (35 mM glycine in H_2O with 1% (w/v) BSA, pH 6.35) and allowed to mix for 30 min at room temperature. The sample was washed and resuspended in storage buffer [10 mg/mL BSA in PBS, pH 7.4] and stored 4°C until use.

2.2.3 Characterization of binding specificity

Binding specificity of covalently coupled CTxB-microspheres to the membrane incorporated ganglioside GM1 controls were conducted (Table 2.1). Fluorescence imaging was used (as described in Section 2.3.6) to assess specificity (Fig. 2.3). These

studies were conducted to: (1) ensure that the microspheres were covalently coupled to the cholera toxin B subunit, (2) visually assess the specificity of the coupled microspheres affinity for GM1 [1.0 mol%], and (3) evaluate that the CTxB-microsphere handles bind specifically to GM1 for optical trapping manipulation. A single species bilayer containing POPC were used for all controls (Fig. 2.3). Negligible levels of microspheres, relative to the positive control (Fig. 2.3a), were seen therefore supporting specific binding between CTxB-microspheres and GM1 in a planar supported bilayer.

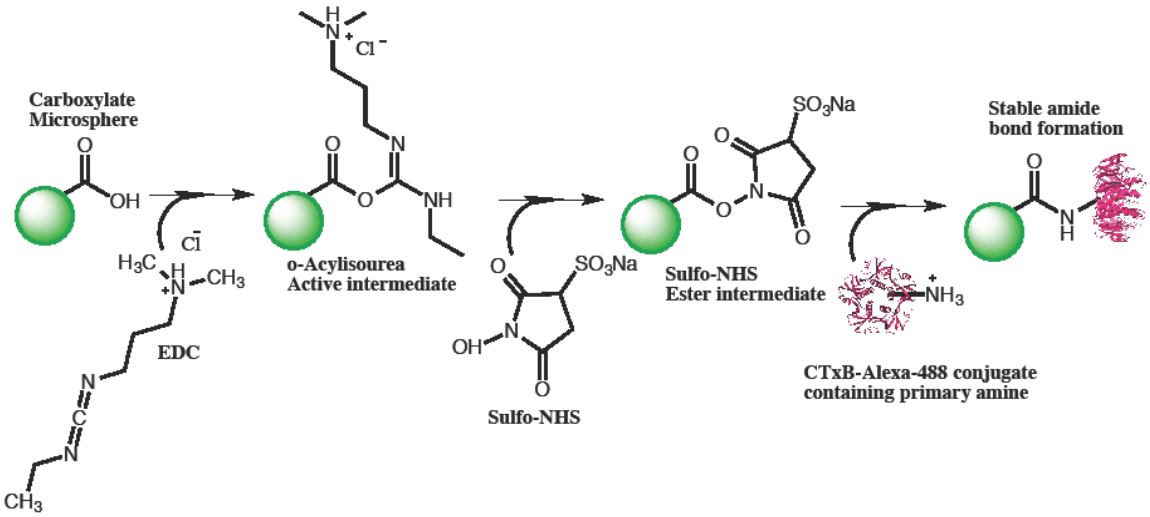

Figure 2.2 Covalent coupling of carboxylate microspheres to cholera toxin B subunit through stable amide bond. Note: not drawn to scale.

Table 2.1. Representative table for controls used for binding specificity experiments.

	a	*b*	*c*	*d*	*e*	*f*
GM1[&]	+	–	+	+	+	–
CTxB	–	–	–	+[^]	+[*]	+
CTxB-Microspheres	+	–	–	+	–	+

^ denotes the use of non-fluorescently labeled cholera toxin B
* represents the use of fluorescent AlexaFluor 488 recombinant cholera toxin B
& signifies the incorporation of 1.0 mol% ganglioside into the bilayer

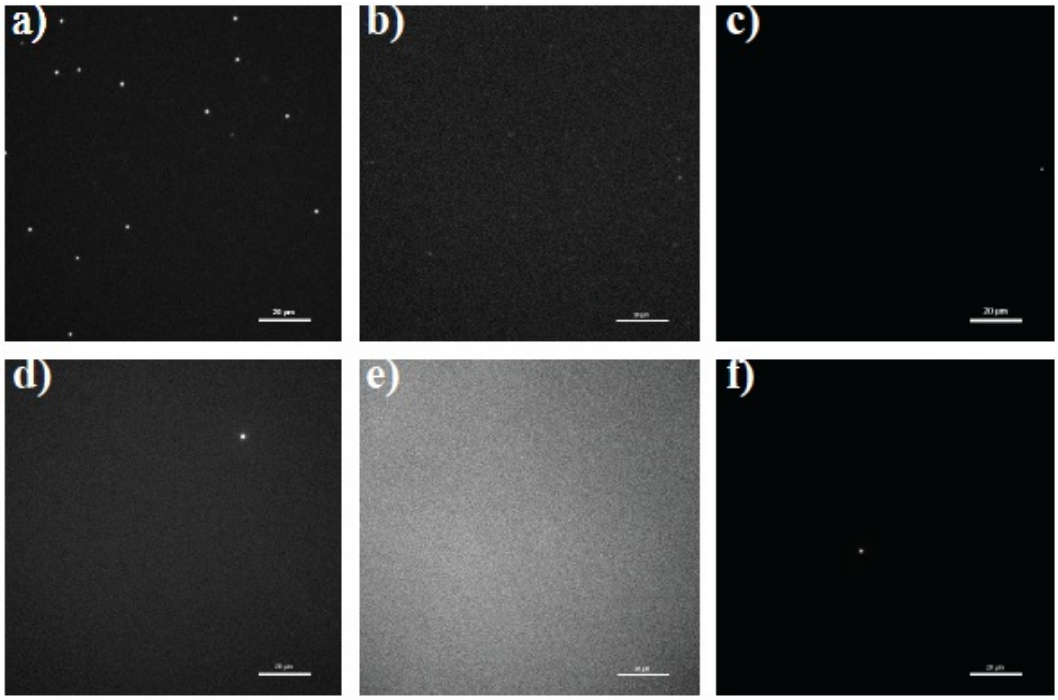

Figure 2.3 Fluorescence images of binding specificity controls. a) Positive control of CTxB-microspheres binding to GM1 incorporated into a POPC planar supported bilayer, b) negative control of a POPC planar supported bilayer, c) 1.0 mol% GM1 incorporated into the POPC bilayer with no treatment with CTxB or CTxB-microspheres, d) uniform binding of non-fluorescent CTxB to block GM1 before treatment with CTxB-microspheres, e) Alexa488-CTxB recombinant to show uniform fluorescence distribution by binding to GM1 and f) negligible levels of binding of CTxB-microspheres without GM1 incorporation. All model membranes contained POPC. All model membranes positive for GM1 contained 1.0 mol% (Table 2.1). Scale bar, 20 μm.

2.3 Materials and methods of optical system

2.3.1 Fluorescence correlation spectroscopy

Madge, Elson and Webb first used fluorescence correlation spectroscopy (FCS) in 1972 for high-resolution spatial and temporal analysis (*58*). It is a minimally invasive technique used in both *in vitro* and *in vivo* applications to investigate particle diffusion, conformational changes, as well as chemical and photophysical reactions (*49, 59-63*). FCS measures spontaneous intensity fluctuations as fluorescent molecules travel through a small observation volume (< 1 femtoliter) caused by deviations from thermal equilibrium. These intensity fluctuations are recorded photon by photon and are quantifiable by strength and duration through autocorrelation to determine local concentration, mobility coefficients, and rate constants (*64*). Autocorrelation is based on self-similarity of the time signal to create characteristic time constants associated with different processes (*64*). The number of molecules (N) in the focal volume is based on a Poisson distribution. Interestingly, the relative fluctuations decrease with the increase in number of particles. Therefore, detection occurs optimally at low concentrations (nM) and is observed through a high numerical aperture (NA) objective (*65*). The time scale for FCS ranges from μs to ms. For our purposes, FCS is used to study deviations from normal homogenous lateral diffusion of fluorescently labeled lipid species (lipid analogs) with biomembranes, and we expand this to bilayers that have optical trap-induced phase separation properties (*48, 66*). This comparison will be distinguishable through single to multiple diffusion coefficients quantified from fitting autocorrelation functions with Levenberg-Marquardt non-linear least square routines (*61*).

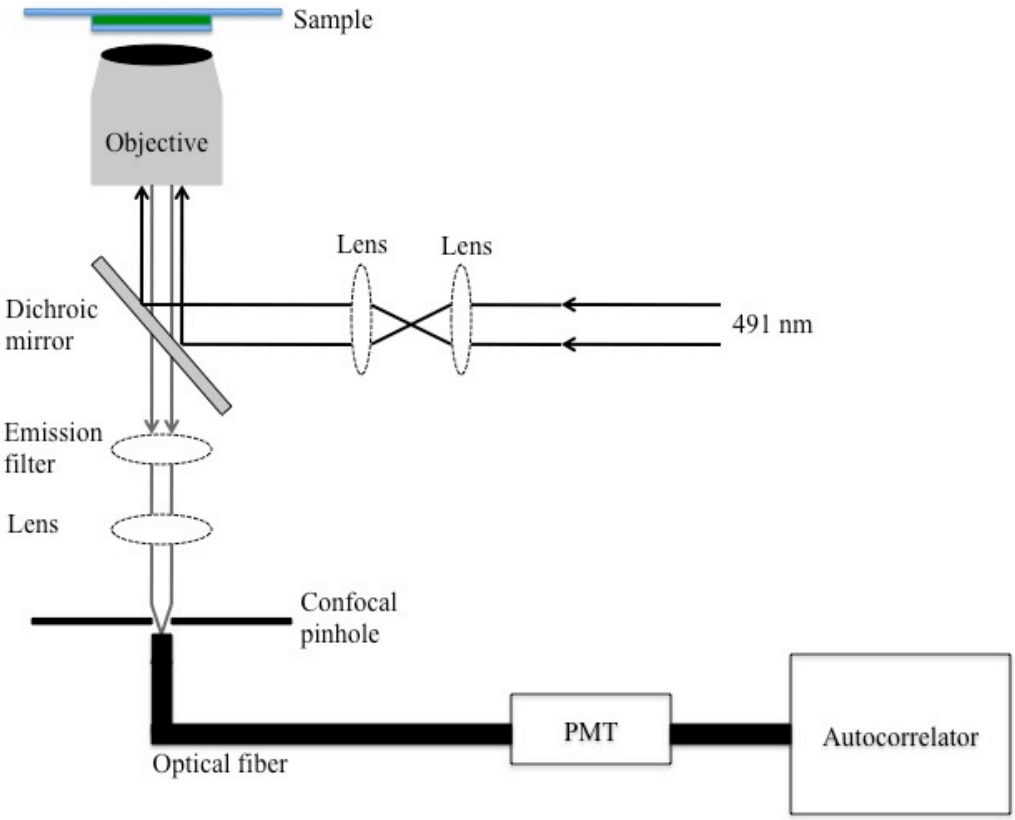

Figure 2.4 Schematic diagram of the excitation and emission path of FCS. The 491 nm incident beam is collimated, expanded and enters the back aperture of a high NA objective to create a diffraction-limited spot at the sample plane. The dichroic mirror acts as a wavelength-dependent beam splitter by reflecting excitation light and transmitting red-shifted light. The emission filter suppresses Rayleigh and Raman scattering and sends signal through optical fiber (25, 50, or 100 μm diameter), which is coupled to a photomultiplier tube (PMT) detector and recorded through the Flex02 acquisition program (Correlator.com).

2.3.2 Theory of FCS

FCS is based on the fluctuation dissipation theorem of statistical physics, which can be described by the linear response theory (*67*). A linear response of a given system, once perturbed, can be expressed as fluctuations of the system in thermal equilibrium (*68, 69*). The underlying concept of FCS is to take a small detection volume, and record the natural fluorescence intensity fluctuations caused, not by a perturbation, but rather the system's thermal motion as molecules pass through this volume (Fig. 2.5b). The point-spread function of the measured fluorescence intensity created by a highly focused laser beam creates a three-dimensional Gaussian. The single photon excitation is displayed as (*70*)

$$I(x,y,z) = I_0 e^{-2\left(\frac{x^2+y^2}{\omega_{xy}^2}+\frac{z^2}{\omega_z^2}\right)} \tag{2.1}$$

where I_0 denotes the maximum intensity created and ω_{xy} and ω_z are the lateral and axial radius of volume, respectively. The fluorescence signal is defined as deviations from the temporal average of the signal over time (*64, 71, 72*) as

$$\delta F(t) = F(t) - \langle F(t) \rangle. \tag{2.1}$$

A small sample size allows for the signal to be autocorrelated by way of an induced time lag to define deviations from the temporal average of the signal. The autocorrelation function is the normalized variance of the fluctuating fluorescence signal δF(t).

$$G(\tau) = \frac{\langle \delta F(t) \cdot \delta F(t+\tau_D) \rangle}{\langle F(t) \rangle^2} \tag{2.2}$$

This diffusion time is then used to determine the translational diffusion coefficient (D_τ).

$$\tau_D = \frac{\omega_{xy}^2}{4D_\tau} \tag{2.3}$$

To acquire dynamic information from the signal obtained from the autocorrelation function, the signal can be written in terms of diffusion time

$$G(\tau) = \frac{1}{N}\frac{1}{\left[1+\left(\frac{\tau}{\tau_D}\right)^{\alpha}\right]}\frac{1}{\left[1+\left(\frac{1}{\omega_0^2}\right)\left(\frac{\tau}{\tau_D}\right)^{\alpha}\right]^{1/2}} \tag{2.4}$$

where:

$$N = V_{eff}C \tag{2.5}$$

$$V_{eff} = \pi^{3/2}\omega_{xy}\omega_z \tag{2.6}$$

$$\omega_0 = \omega_z/\omega_{xy} \tag{2.7}$$

N is the average number of molecules in the observation volume, V_{eff} is the effective detection volume, C represents the concentration and α denotes the anomalous exponent for conventional Brownian motion and α<1 for non-Brownian motion (*73*). ω_0 represents the structural parameter. G(0) is inversely proportional to N within the detection volume due to the assumption of a Poisson distribution.

2.3.3 Characterization of the FCS system

The FCS system was initially characterized and aligned using rhodamine green (5[6]-carboxyrhodamine 110 [Marker Gene Technologies]) in solution (Fig. 2.6). For these experiments, the concentration of rhodamine green was 0.5-2 nM in PBS (pH 7.4) buffer (Fig. 2.7a). A 491 nm Cobolt Calypso 100 laser, Plan APO 60 × 1.2 NA water immersion objective on an inverted Nikon Eclipse T*i* scope, Semrock Brightline LF 488/ LP-B-NTE filter, and 0.54 neutral density (ND) filter were used for characterization (Fig.

2.7). The optical fiber diameter varied (25, 50, 100 μm). Two Hamamatsu GaAsN single photon counting PMTs were used for detection. Correlation was carried out with a 60 s acquisition time using the Flex02 software (correlator.com). IgorPro (Wavemetrics) and Origin software (OriginLab) was used for all rhodamine green characterization experiments. Fitting was assessed based on chi squared (χ^2) goodness of fit statistical analysis (Fig. 2.6).

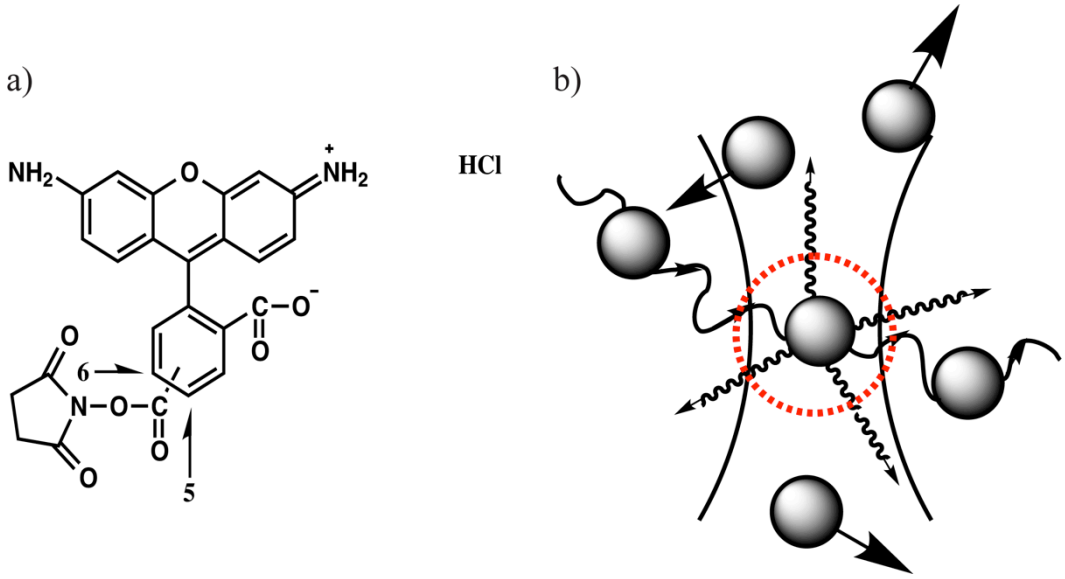

Figure 2.5 Rhodamine green structure and representative observation volume for detection. As a a) rhodamine green molecule passes through the b) observation volume, it is excited. The intensity fluctuations are recorded by a PMT detector and used for FCS acquisition. The dimensions of the observation volume are defined by ω_{xy} and ω_z.

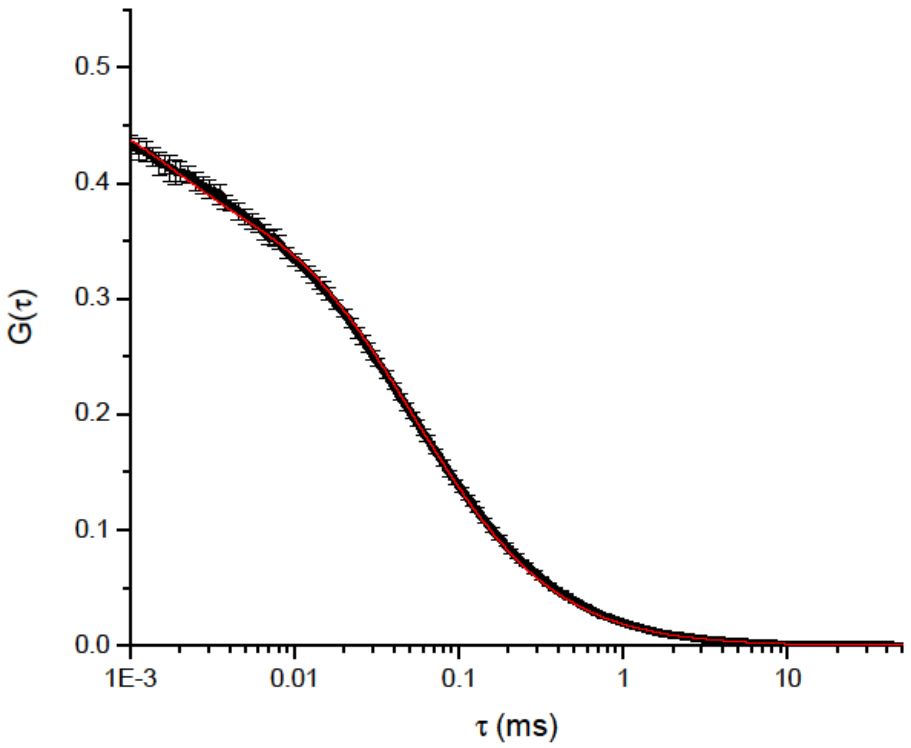

Figure 2.6 Representative rhodamine green autocorrelation curve (*n = 18*). The bars represent ± SD, and fitting was based on χ^2 best fit in three dimensions (*58*). Rhodamine green was used as a control for all FCS studies to calculate the diffusion coefficient of lipid species based on the experimental τ_D of rhodamine green and its known $D = 2.8 \times 10^{-6}$ cm^2/s.

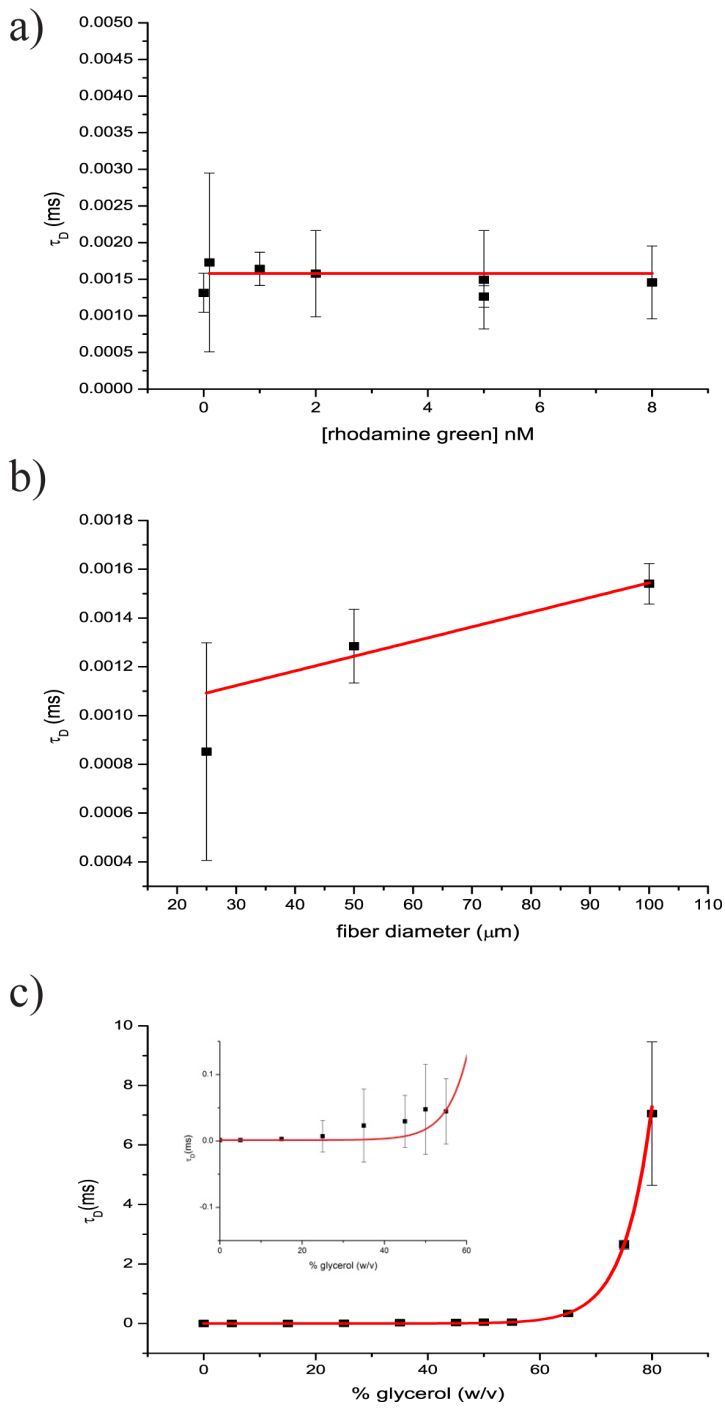

Figure 2.7 Characterization of FCS system with rhodamine green. For all curves, error is ±SD associated with calculated τ_D calculated from autocorrelation function (Eq. 2.4). a) By varying [rhodamine green] τ_D is constant, as seen with the linear fit analysis. b) By varying the optical fiber diameter τ_D increases proportionally and linearly. c) By varying the viscosity of the local environment τ_D increases exponentially. Inset shows addition of glycerol < 60% (w/v). Each point corresponds to *n=9*.

Diffusion studies of rhodamine green in solution show the following: 1. There is no dye concentration dependence on diffusion time, which is expected for a monomeric dye in solution (Fig. 2.7a). 2. There is a linear dependence on τ_D on the fiber diameter, which defines ω_{xy} as described in Eq. 2.3 (Fig. 2.7b). 3. As viscosity increases by increasing the percent glycerol, τ_D also increases (Fig. 2.7c). The Stokes-Einstein model describes the relationship in which diffusion is dependent on the radius of a spherical particle (a), Boltzmann's constant (κ_B), temperature (T), and the dynamic viscosity of the local environment (η).

$$D = \frac{\kappa_B T}{6\pi\eta a} \tag{2.10}$$

Taken together, these results demonstrate that our FCS system is well-calibrated.

2.3.4 Optical trapping

Optical trapping is a technique that takes advantage of the wave-particle duality of light to manipulate the locality of nanoparticles in biomimetic and biological systems (*48, 74*). When light is tightly focused through a high NA objective, the strong electric field creates an optical force. The momentum created by photons is used to generate a parabolic force potential well where particles spanning nm-µm in size can be physically trapped and subsequently manipulated in three-dimensions (*75*). Introducing a differential optical element, such as a spatial light modulator (SLM) allows for the multiple traps to be controlled in real-time from a single light source (*76, 77*). The introduction of this element is referred to as a holographic optical trap (HOT). The inclusion of multiple traps from a single light source allows for the manipulation of

several components simultaneously. This technique is beneficial in studying the interaction of multiple biomolecules through this mechanical manipulation.

2.3.5 Theory of optical trapping

The theory can be described by three alternative regimes (Rayleigh, generalized Lorenz-Mie and Mie). For our purposes, the Rayleigh regime (Fig. 2.10) best describes our optical approach due to the wavelength of the infrared laser (1064 nm) acting on a particle of a smaller diameter (0.97 μm). The two forces that are created by the photons reflecting and refracting off the particle being trapped are called scattering and gradient forces. The gradient force generates the potential trapping well,

$$F_{grad} = \frac{\beta}{2} \nabla \langle E^2 \rangle \tag{2.11}$$

whereas the scattering force is in the direction of laser propagation (*78*).

$$F_{scatt} = n_m \frac{\langle S \rangle \sigma}{c} \tag{2.12}$$

The scattering force actually pushes the particle out of the well to produce a trap, $F_{grad} > F_{scatt}$. The magnitude of the force we can exert on a particle is dependent largely on particle size (r), refractive indices of the particle (n) and surrounding medium (n_m), and the intensity of our laser that creates the gradient of electric field (E). β is combined relationship between particle size and the ratio of refractive indices of the particle to that of the surrounding medium.

$$\beta = n_m^2 r^3 \left(\frac{m^2-1}{m^2+2}\right) \tag{2.13}$$

The cross-sectional area of the Rayleigh sphere (σ) and the time averaging Poynting vector (<S>) influence F_{scatt}.

$$\sigma = \frac{8}{3}\pi(kr)^4 r^2 \left(\frac{m^2 - 1}{m^2 + 2}\right)^2 \tag{2.14}$$

$$k = \frac{2\pi n_m}{\lambda} \tag{2.15}$$

$$m = \frac{n}{n_m} \tag{2.16}$$

Essentially, dielectric particles are attracted along the gradient to regions of strong electric field by way of the conservation of momentum. To date, we have implemented the use of a single wavefront optical trap, with our efforts focused on creating a holographic optical trap to manipulate multiple microspheres simultaneously in real-time.

2.3.6 Holographic optical trapping

Our system contains the necessary components to enable a holographic optical trap (HOT) to better study biomolecular interactions (Fig. 2.10). These components include a Laser Quantum Ventus 1064 model infrared laser, combined with a Boulder Non-linear Systems 512-15 Flex Rev. 1.0 spatial light modulator (SLM) by way of a Nikon Eclipse T*i* inverted scope platform containing a Plan APO 60 × 1.4 NA oil immersion objective (Fig. 2.9). The HOT is achieved through PCIe Devices LabVIEW computer software to generate a desired trapping arrangement where a hologram is displayed at the SLM. Video acquisition is obtained using a Photometrics Evolve electron-multiplier charged-coupled device (CCD) camera with Nikon Elements

software. A X-Cite Series 120 Q lamp is used for wide field epi-fluorescence and a 485DF/15 exciter wheel in combination with the Omega Optical XF 2050 dichroic and XF 3063 emitter filters for imaging. A desired trapping arrangement is generated through a pixel array to polarize liquid crystals to generate multiple wavefront beams from a single light source. The SLM is a Fourier pair with the objective that transforms the hologram at the sample plane.

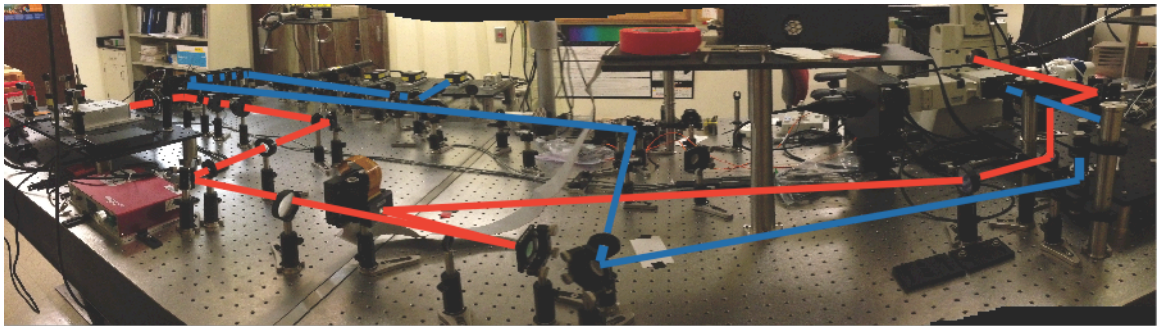

Figure 2.8 Multimodal integrated optical set up on a single platform that allows for the measuring of lateral diffusion with FCS (blue) and mechanical control of biomolecules through optical trap (red).

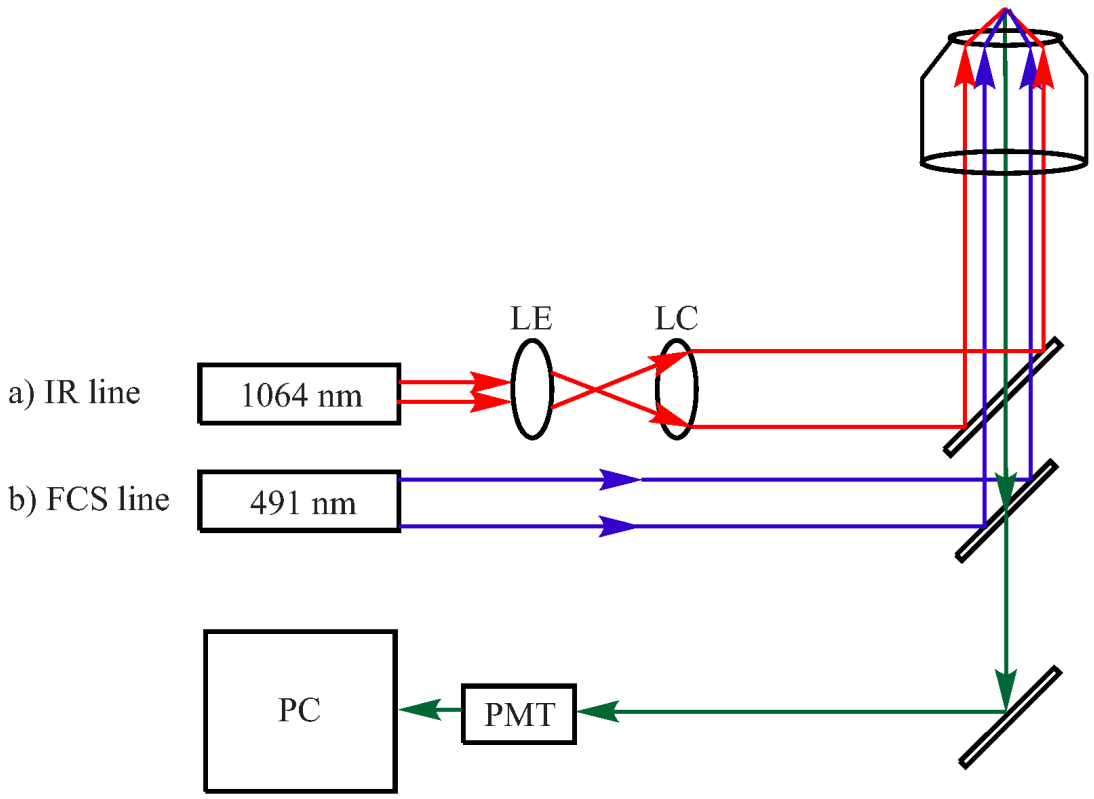

Figure 2.9 Schematic of components of single platform system for the manipulation of membrane domains. a) The optical trap laser line is a 1064 nm IR laser that has passed through a beam expander and collimator to a Nikon CFI Plan APO 60 × 1.4 NA objective. b) The 491 nm Cobolt Calypso 100 laser is used to illuminate samples and collect fluorescence fluctuations of excited fluorophores through a Semrock 670 nm BrightLine Multiphon SWP dichroic mirror by way of a PMT detector.

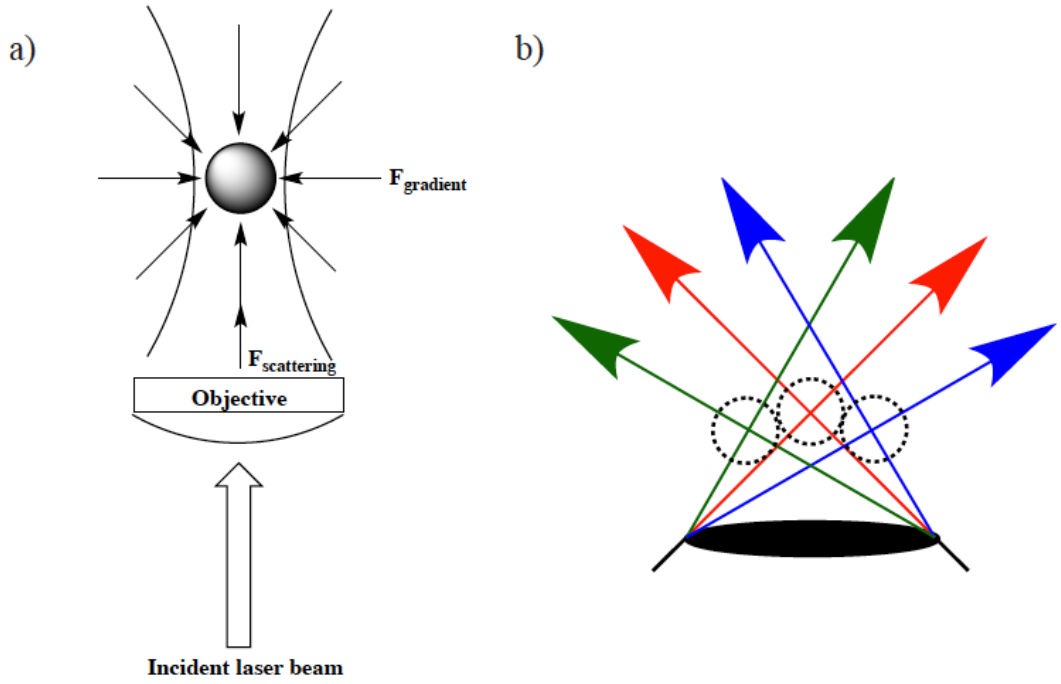

Figure 2.10 Optical trapping in the Rayleigh regime. a) An incident beam creates gradient forces that trap the microsphere and scattering forces that push the microsphere in the direction of the beam b) objective displaying multiple traps from a single light source, HOT system approach, created by the implementation of an SLM.

III: Characterizing the mobility of phospholipids as a function of GM1 concentration in the planar bilayer

Understanding the underlying effects of incorporating various concentrations of GM1 is of utmost importance when optimizing our model system for optical trapping. In this Chapter, the effects of GM1 concentrations on the lateral diffusion of the incorporated fluorescent lipid analog NBD-PC in POPC planar supported bilayers is quantitatively measured with FCS. The ability to optically trap CTxB-microspheres in various concentrations of GM1 will be addressed. All optical trapping experiments were conducted with Tyler Floden of the University of Minnesota, Duluth.

3.1 Background

Recent work has focused on understanding the physiological role of GM1 in the prevention of membrane-mediated diseases (*79-81*). The bulky headgroup of GM1 contains several sialic acid residues joined together by α-glycosidic linkages (Fig. 1.4). GM1 is found predominantly in the outer leaflet of the plasma membrane, particularly in neuronal membranes (*82*). GM1 has been shown to play a significant role in cell signaling, adhesion, sorting, and recognition (*79, 80*). In the case of Huntington's disease, a neurodegenerative disorder caused by polyglutamine expansion in the huntingtin protein, a disruptive mechanism for GM1 production leads to an increased susceptibility to apoptosis (*83*). The resulting inhibition of GM1 production is thought to play a significant role in Huntington's disease (*83*).

The importance of GM1 resides in its ability to stabilize S_o phase lipid microdomains (*79, 84*). The incorporation of GM1 in model membranes of lipid

compositions containing DOPC/SM/cholesterol mixtures (59:36:15 mol%), compositions chosen to mimic mammalian plasma membranes, has been shown to create GM1 localization in domains (*84*), which is thought to be due to the hydrogen bonding between GM1 and SM. The addition of cholesterol has an interesting implication in the previously described ternary mixture. Cholesterol disorders tightly packed S_o regions created by SM and orders L_α regions of DPPC (*84*), leading to the liquid-ordered phase. When cholesterol interacts with PC, it has an ordering and condensing effect (*85*). Due to the tilt of the sterol ring, it orders hydrocarbon chains and creates condensed membrane packing (*85*). SM, due to its amide, carbonyl, and hydroxyl functional groups (Fig. 1.2) allows for hydrogen bonding to occur with cholesterol to induce a preferential ordered and condensed interaction relative to PC (*85*). The L_o phases comprised of SM and cholesterol contain twice as many hydrogen bonds as that of cholesterol and PC, which in addition to charge pairs between choline groups and van der Waals interactions generates phase separation (*85*). The interaction between GM1 and cholesterol in L_o regions induces a conformational change (*85*). GM1's carboxyl group and choline group in PC also form a charge pair (*85*). Understanding these preferential interactions is the foundation for our investigations in membrane structure and organization.

We are particularly interested in understanding preferential membrane organization that leads to domain formation marked by the presence of GM1. Due to the low T_m of both DOPC and POPC, they are used interchangeably in model systems to create similar lipid phase behavior diagrams (*84*). The structure of GM1 is thought to play a role in this segregation and stabilization of membrane domains (*79*). GM1 has the

capability to create a network of hydrogen bonding at the water-lipid interface, as well as to play a substantial role in membrane reorganization through its long, saturated acyl chains (*79*). These factors create its preferential association with SM and cholesterol, that is, L_o regions of model membranes. It is this favored relationship that we are most interested in understanding by inducing interactions with HOT and studying the subsequent dynamics with FCS.

Studies have shown a wide range of conflicting values characterizing the influence of GM1 on the lateral mobility of various phospholipids (*80, 81*). The experiments described in this Thesis pertain to POPC planar supported bilayers, with the incorporation of various concentrations (0, 0.05, 0.1, 0.5 and 1.0 mol%) of GM1. Physiologically relevant GM1 concentrations on the plasma membrane outer leaflet range from 0.5 to 5 mol% (*80*). Several factors are thought to play an influential role in the varied phospholipid mobility due to [GM1] such as, lipid type and composition, cholesterol content, influence of CTxB binding, and GM1 headgroup interactions (*80, 81, 84*).

Previous studies have used fluorescence recovery after photobleaching to quantify the translational diffusion of fluorescent phospholipid species (*80, 81*). In these cases, higher levels (1.0 mol%) of lipid analogs were used, which due to their charged and relatively large headgroups (e.g., TexasRed-DHPE) are thought to interact directly with GM1, subsequently increasing the diffusion. GM1 contains a headgroup that covers an area of 21 $Å^2$ from the hydrocarbon-water interface, as determined using quartz crystal microbalance with dissipation monitoring (*80, 81*). This headgroup protrusion is thought

to influence lateral diffusion of lipid species. To better understand the role of GM1 and its influence more broadly on lipid lateral diffusion, we constructed fluid POPC supported bilayers and used the fluorescent lipid analog, NBD-PC that contains an acyl chain-labeled fluorophore to potentially eliminate the effects of headgroup interactions (Fig. 2.1). In characterizing an adequate concentration of GM1 to mechanically manipulate CTxB-microspheres, we analyzed the influence of CTxB (*81*) as well as the influence of our CTxB-microspheres when bound. FCS allows us to quantitatively assess fluorophore fluctuations and its effects on lateral diffusion at very low fluorosphore concentrations (0.1 mol%), which also minimizes potential disruptive packing effects of the fluorophore.

Single-molecule techniques such as FCS can be used to obtain the characteristic D of the fluorophore and the average number of molecules (nM concentration) in the observation volume (for a diffraction-limited spot) (*71, 86, 87*). FCS allows us to study lateral diffusion allows us to quantitatively assess fluorophore fluctuations at very low concentrations (0.1 mol%), which also minimizes potential disruptive packing effects of the fluorophore (*88*). These techniques allow us to quantitatively investigate the distributions and dynamics of molecules within biomimetic membranes and living cells.

3.2 Results and discussion

Effects of [GM1] on lateral diffusion of lipid analog, NBD-PC in planar supported bilayers

Previous work investigated the impact of saturated DMPC bilayers at slightly above the phase transition (T_m = 24.5 ºC) containing 1, 5 and 10 mol% [GM1] with a diI-derivative lipid analog (*81*), noting D = 1.1 × 10^{-8} cm^2/s for lipids containing no GM1 and D = ~ 2.0 × 10^{-9} cm^2/s for lipids containing the various [GM1] (*81*). In a more recent study, unsaturated egg yolk L-α-phosphatidylcholine (egg PC, T_m = −15 ºC) was used in addition to 1.0 mol% TexasRed-DHPE lipid analog in supported membranes at 25 ºC (*80*). These membranes contained 2 or 5 mol% [GM1], and the corresponding lateral diffusion for 0, 2, 5 mol% was D = (1.58, 1.44, and 1.32) × 10^{-8} cm^2/s, respectively (*80*). In more biologically relevant systems, methods such as single particle tracking are used to quantify the mobility of specifically labeled species with 40 nm ligand coated colloidal gold nanoparticles (*89*). GM1 in live cells underwent similar lateral diffusion to that of GPI-anchored protein Thy-1 in terms of confinement and diffusion (*89, 90*). The lateral diffusion coefficient of GM1 ranged from × 10^{-10} – × 10^{-12} cm^2/s, whereas their lipid analog (N-(5-fluoresceinthiocarbamoyl)-1,2-dihexadecanoyl-*sn*-glycero-3-phosphoethanolamine) displayed D = 5.6 × 10^{-10} – 0.15 × 10^{-11} cm^2/s, ranging from fast to stationary movements at a 6.6 s time scale in planar supported bilayers determined by single particle tracking (SPT) (*89*).

Our results indicate the same trend in GM1's ability to increase the lateral diffusion time. In POPC bilayers containing 0.1 mol% of NBD-PC, we determined D = $(5.25 \pm 0.12) \times 10^{-8}$ cm^2/s (*n = 18*) in the absence of GM1, and at 1.0 mol % GM1, we observed a reduced value of D = $(2.7 \pm 0.06) \times 10^{-8}$ cm^2/s (*n = 19*; Table 3.1, Fig. 3.1). These diffusion coefficients are consistent with the attenuation of lateral diffusion by the presence of GM1 in the bilayer as observed by others in the literature (*80, 81, 89*). At lower concentrations of GM1 (0.01, 0.1 and 0.5 mol%), we observed minimal effects of GM1 on lateral diffusion of NBD-PC. A possible explanation for the uncharacteristic lateral diffusion trend at 0.1 mol% GM1 could be due to partitioning of the NBD-PC lipid analog in different leaflets of the bilayer, therefore influencing the lateral diffusion by substrate effect (Fig. 3.1).

Impact of CTxB binding on various [GM1] on lateral diffusion of NBD-PC in planar supported bilayers

Earlier work indicated that the presence of bound CTxB (1.0 μg/mL) decreases the diffusion coefficient of lipid species by a very small amount (*81*). Our work supports this finding at saturating concentrations assessed with fluorescence intensity consistency. Figure 3.2 shows this decrease in lateral diffusion. We observe a decrease in the lateral mobility of NBD-PC as we increased [GM1]. This result is not surprising perhaps because CTxB contains five binding sites for GM1, which likely influence the redistribution and resulting GM1-GM1 interactions that may ultimately create a network to reduce diffusion of the surrounding lipid species (that is, our NBD-PC diffusive

tracer). The lateral diffusion of CTxB (0.1 μg/mL) has been shown with fluorescence recovery after photobleaching and SPT to be $D = 1.2 \pm 0.3 \times 10^{-9}$ cm^2/s after a crosslinking event (*91*). Unfortunately, the diffraction limit of light (< 200 nm) limits our ability to qualitatively assess the lipid heterogeneity of proto-rafts before an induced cross-linking event (*91*).

Consequence of CTxB-microsphere binding to GM1 on lateral diffusion of NBD-PC in planar supported bilayers and CTxB-microsphere mobility has an effect of GM1

To test the influence of our CTxB-microsphere handle for future optical trapping experiments, we assessed the lateral mobility of our lipid analog in the presence of bound CTxB-microspheres. Our results suggest that the influence of CTxB-microspheres does decrease the mobility of our lipid analog as a whole, similar to that of CTxB not covalently coupled to microspheres (Fig. 3.2). We see a decrease in lateral diffusion from $(5.25 \pm 0.12) \times 10^{-8}$ cm^2/s ($n = 18$) under conditions of no beads or GM1 present to $3.96 \pm 0.09) \times 10^{-8}$ cm^2/s ($n = 16$) at GM1 of 1 mol% concentration (Table 3.1).

We were able to assess the mobility of our bound CTxB-microspheres qualitatively with fluorescence imaging. We observed a range of CTxB-microsphere mobility apparent with time lapse video imaging, which we hypothesize is due to the degree of binding occurring at each CTxB (based on quantity of occupied binding sites). At concentrations of 0.5 mol% and greater GM1, we do not observe mobility of the CTxB-microsphere. At 0.05 mol% GM1, we observed the greatest degree of lateral motion of CTxB-microspheres. By analyzing the lateral mobility of CTxB-microspheres,

we were able to determine the optimal GM1 concentration to optically manipulate CTxB-microsphere handles.

Effects of [GM1] on lateral movement of optically trapped CTxB-microspheres

We hypothesize that the ability to control the degree of lateral mobility of our CTxB-microsphere handle is influenced by the number of occupied binding sites per CTxB with GM1. During time-lapse imaging, varied levels of mobility were depicted dependent on [GM1]. CTxB aggregation upon binding to GM1 has been studied (*92*), but through qualitatively fluorescence imaging, wed did not observe aggregation under low GM1 concentrations (< 0.5 mol%). CTxB-microspheres were uniformly and randomly dispersed across the bilayer. Interestingly, we were able to qualitatively assess the mobility of 0.05 and 0.1 mol% [GM1], but mechanically manipulate microspheres only when membranes contained 0.05 mol% GM1. We hypothesize that further optimization of our laser power efficiency for the optical trap and a decrease in the microsphere diameter will allow us to create a broader spectrum of more physiologically relevant GM1 concentrations for mechanical manipulation.

FCS and fluorescence imaging techniques provide a platform for model system optimization

A decrease in the lateral diffusion of our lipid analog, NBD-PC is evident at GM1 incorporation levels greater than 0.5 mol%. CTxB and CTxB-microspheres binding to GM1 at various concentrations has shown to decrease the lateral diffusion of NBD-PC in

planar supported bilayers (Fig. 3.1). Our ability to optically trap and manipulate CTxB-microspheres in the *xy* plane is limited to low GM1 concentrations (0.05 mol%). The results gained from FCS controls give us insight as to the dynamics of underlying lipid species involved in reorganization as we increase the complexity of our model system.

Table 3.1 Lateral diffusion of 0.1 mol% NBD-PC in POPC (Tm -2 ºC) bilayers containing varying amounts of [GM1].

	D (× 10^{-8} cm^2/s)		
[GM1] (mol%)	***– CTxB – CTxB-microspheres***	***+ CTxB – CTxB-microspheres***	***– CTxB + CTxB-microspheres***
0	5.25 ± 0.12 (*n = 18*)		
0.05	5.32 ± 0.11 (*n = 15*)	4.67 ± 0.09 (*n = 15*)	4.34 ± 0.09 (*n = 19*)
0.1	9.35 ± 0.21 (*n = 13*)	4.67 ± 0.10 (*n = 13*)	2.84 ± 0.04 (*n = 19*)
0.5	6.17 ± 0.15 (*n = 16*)	3.40 ± 0.06 (*n = 16*)	6.00 ± 0.13 (*n = 19*)
1.0	2.70 ± 0.06 (*n = 19*)	3.04 ± 0.06 (*n = 19*)	3.96 ± 0.09 (*n = 16*)

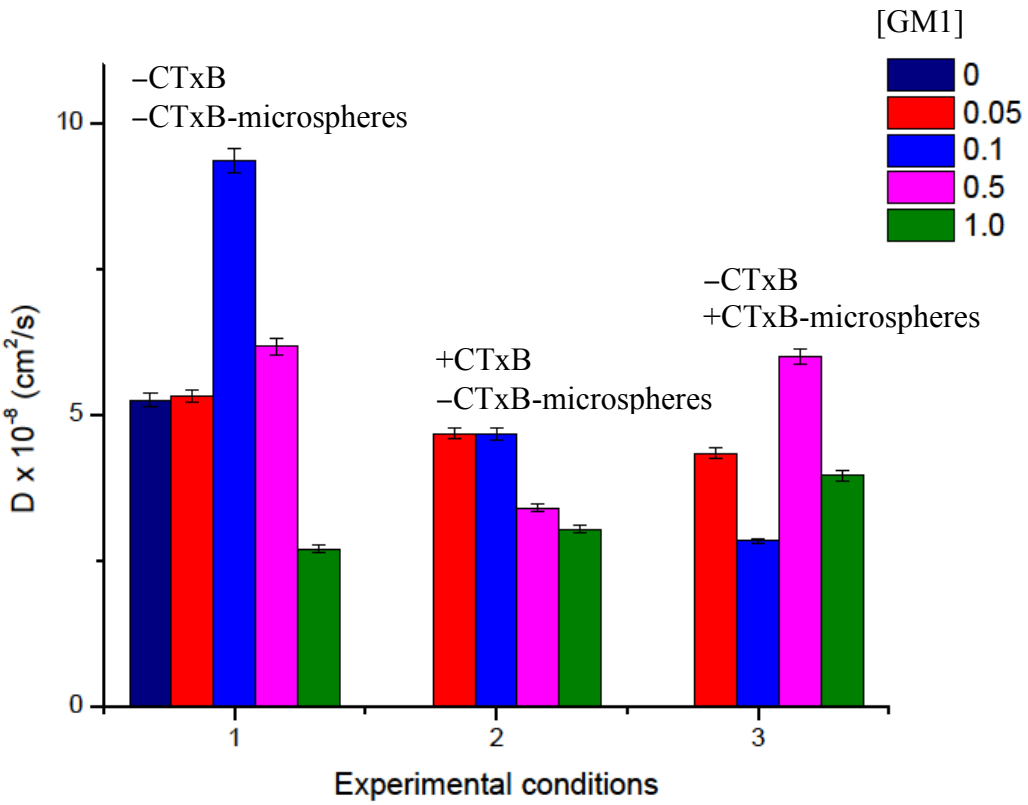

Figure 3.1 Graphical depiction of lateral diffusion coefficients of 0.1 mol% NBD-PC in POPC bilayers containing varying amounts of [GM1]. Experimental conditions 1) bilayer in the absence of CTxB and CTxB-microspheres, 2) in the presence of non-fluorescent CTxB and 3) in the presence of CTxB-microspheres. Error bars indicate ± SD.

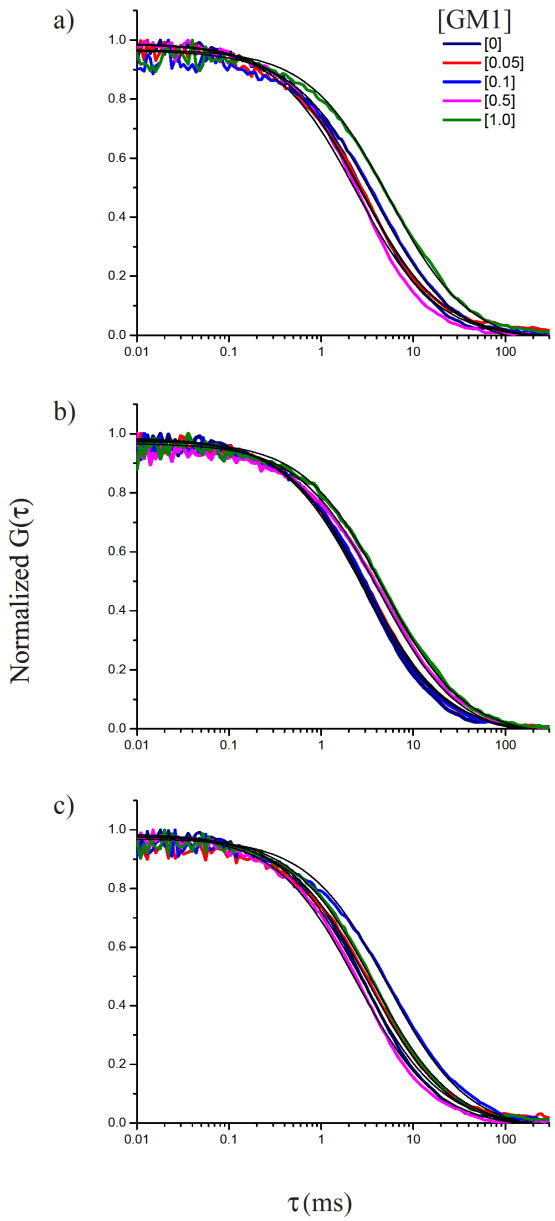

Figure 3.2 Normalized autocorrelation curves depicting lateral diffusion of varying [GM1] in a POPC bilayer containing 0.1 mol% NBD-PC. Fit functions correspond to Eq. 2.6. a) Depicts conditions of no CTxB, b) non-fluorescent CTxB and c) CTxB-microspheres bound.

IV: Nucleation of cholesterol-rich domains using light as a "crosslinking ligand"

This Chapter will describe our progress of implementing optical trapping in our multimodal imaging system (*48*), which allows us to non-invasively and dynamically manipulate biomolecules (lipids, proteins) that are conjugated to nanoparticles (e.g., colloidal gold, quantum dots, and polystyrene microspheres), while simultaneously performing imaging or dynamic measurements with FCS. Tyler Floden, of the University of Minnesota Duluth, customized, optimized, and calibrated the optical trapping system used in this Thesis.

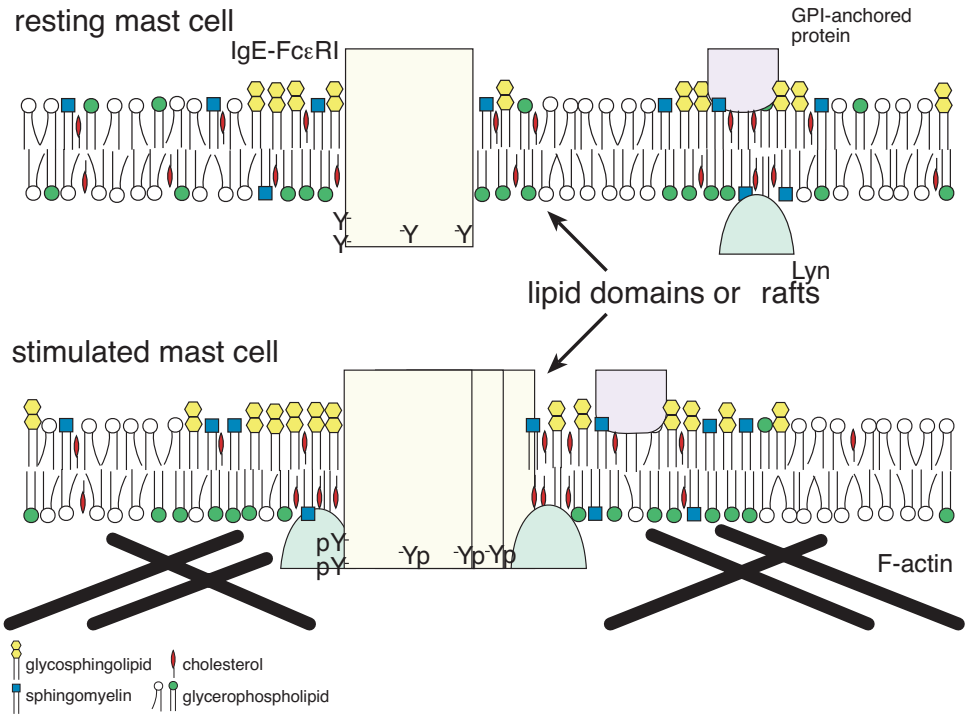

Figure 4.1 Cholesterol-mediated signaling of the IgE receptor (FcεRI). In resting mast cells, the IgE receptor weakly associates with cholesterol-rich nanodomains to form a "proto-raft". Acylated (e.g., the Src kinase Lyn) and lipid-anchored proteins are more strongly associated with these microdomains. Upon crosslinking with a multivalent antigen, the proto-rafts coalesce, transiently, to facilitate the tyrosine phosphorylation of the IgE receptor by Lyn.

4.1 ***Background***

Transient compartmentalization and the resulting molecular interactions in biomembranes must control biological function; however, the field currently lacks the tools to probe the dynamics of these interactions on living cells. In addition, the complexity present in cells poses substantial complications for interpreting the molecular basis of functional interactions occurring *in vivo*. Unfortunately, it has proven difficult to manipulate induced interactions (e.g., crosslinking events) *in vivo* that would give insight into membrane organization at the molecular level. Therefore, novel methods are needed to understand the mechanisms driving reorganization that lead to biological function (*93*).

We hypothesize that the structure and dynamics of cholesterol-rich lipid domains in the plasma membrane facilitate functionally important interactions in immunoreceptor signaling, and our ultimate longterm goal is to understand how membrane structure controls both early (e.g., triggering) and late (e.g., exocytosis) events in mast cell signaling (Fig. 4.1). One hypothesis is that proto-domains exist transiently in biomembranes and as a result of a trigger (e.g., ligand binding to a cell surface receptor), a larger raft nucleates to facilitate the desired function (e.g., signal initiation) (*94*).

We are developing new tools that will allow us to investigate quantitatively the relationship between proteins and lipids in immunoreceptor signaling and their dynamics with high spatial and temporal resolution. Importantly, our work will be directly applicable to other signaling processes that are facilitated by membrane domains. Because crosslinking of the IgE receptor is essential for the initiation of the allergic response, we will mimic this crosslinking using dynamic HOT to nucleate domains in a

dynamic manner; that is, we will use light as our "crosslinking ligand". In an optical trap, optical forces from a focused laser beam are used to manipulate selected components that have been specifically labeled with a colloidal gold, latex or silica nanoparticle (*95*). Previous experiments on biomembranes have used single- or dual-beam traps. Here, we will use dynamic HOT, which can create many traps in user-defined patterns from a single trapping laser, using a computer-controlled spatial light modulator (*96-99*). The individual traps can be uniquely and individually controlled in real-time to manipulate particles within any given pattern. The dynamic HOT will allow for impromptu molecular manipulation, so that we can probe the underlying mechanisms behind the heterogeneities in lateral diffusion and membrane structure. Such spatially controlled manipulation of the membranes will be visualized by fluorescence imaging. Further, temporally resolved dynamics will be measured using FCS (as described in Chapter 2 of this Thesis), single particle tracking, fluorescence anisotropy and fluorescence lifetime.

Dynamic HOT will be used to force nucleation of domains and follow the molecular dynamics of their formation. We will overcome problems associated with crosslinking at the molecular level by using light (optical trapping) to crosslink proto-domains in a well-controlled, yet non-invasive manner. Initially, we are incorporating the ganglioside GM1 in trace amounts (< 0.5 mol%) within supported planar bilayers that are composed of a domain inducing composition (POPC:SM:cholesterol) (e.g., *100, 101, 102*) or into gel phase (e.g., DPPC) and fluid phase (e.g., POPC) controls. The GM1 will form proto-domains within the supported bilayer. By using a domain-specific fluorescent

probe or fluorescently labeled cholera toxin B (conjugated to a trappable microsphere) or GM1, we will assess lateral mobility with FCS and single particle tracking, and rotational mobility with polarization anisotropy. Our approach (as described Chapter 2 of this Thesis) demonstrates the preliminary implementation of our quantitative and qualitative method to mechanically and molecularly assess the formation of domains in a non-invasive manner using a combination of optical trapping and fluorescence correlation spectroscopy. The application of this multimodal system will lead to a better understanding of lipid domain formation, dynamics and their role in IgE receptor (and other membrane protein) signaling.

We are using polystyrene microspheres (or in later experiments, colloidal gold nanoparticles) that have been conjugated to cholera toxin B (*89*) (as described in Chapter 2 of this Thesis) and subsequently allowed to bind specifically to GM1, similar to what has been done for single particle tracking studies on model membranes and cell surfaces (*89*). The colloidal gold or polystyrene microspheres serve as our "handles" for the optical trap. We will then drag the specifically bound GM1-CTxB-microsphere to measure the effects of crosslinking time and force needed to form stable domains. Studies have been conducted assessing phase separations in simple model systems containing limited number of species, described here in this Thesis with POPC:SM:cholesterol (47:23:30 mol%) (*28*). We will then systematically vary lipid composition to assess the crosslinking time and force on domain nucleation. Gel and fluid phase controls, where no domains are expected to form, are critical for interpretation of these experiments. Under the same experimental conditions, subsequent

dynamics can be assessed through FCS to gain insight on the underlying lipid species involved in this reorganization. Fluorescence imaging is a tool that we use to monitor the locality of our trap and fluorescently labeled species.

4.2 Results and discussion

Our objective is to understand the physico-chemical bases behind crosslinking-induced domain formation using quantitative microscopy and spectroscopy. Our long-term goal is to understand how the interactions between lipids and proteins lead to biological function in living cells; however, it is critical to first establish the validity of our experimental approach. This project is designed to elucidate the relationship between membrane heterogeneity and function in biomimetic model membranes.

Implementation of multimodal optical trapping and FCS system

To date, we have built a simple single-beam optical trap, which has trapped individual 0.8 μm silica microspheres and are adding a HOT to trap multiple particles. Our 1064 nm laser at 30% power output has approximately 10 mW through the high NA objective at the sample plane. We are calibrating the trapping potential by applying Boltzmann statistics to the position measurements of a trapped particle (*103*). We are currently optimizing the HOT algorithms used to calculate and generate the holograms that are projected onto the liquid crystal display of the spatial light modulator. The spatial light modulator is located in a plane conjugate to the back focal plane of the objective. The holograms are thus essentially Fourier transforms of the desired trapping

pattern at the image plane. HOT allows us to manipulate, in real time, nanoparticle-labeled molecules in biomembranes. Our recent results support the feasibility of the studies on biomembrane domain nucleation dynamics using HOT in combination with fluorescence correlation spectroscopy (FCS).

Mechanical manipulation of CTxB-microspheres with optical trap in POPC planar supported bilayer

Our initial approach was to assess the ability to manipulate CTxB-microspheres in a single component POPC bilayers containing various GM1 (0.05, 0.1, or 0.5 mol%). Lateral mobility of CTxB-microsphers was qualitatively assessed with fluorescence imaging. An higher-level of bound CTxB-microsphere movement was seen at 0.05 mol% to that of 0.1 mol% GM1 and no mobility of CTxB-microsphere was seen at 0.5 mol% GM1 with time-lapse imaging. By limiting the incorporation of GM1, we observed an increased mobility of bound CTxB-microsphere in POPC model membranes. We were able to manipulate the lateral location of CTxB-microspheres bound to GM1 (0.05 mol%) with an optical trap in the *xy* plane (Fig. 4.2). Upon release of the optical trap, CTxB-microspheres retained their position in the *z* plane, supporting the proof of concept that CTxB-microsphere remained bound to GM1 after manipulation with the optical trap. Therefore, optically trapping and manipulating a bound CTxB-microsphere's lateral position within the membrane does not interfere with binding to the GM1 receptor.

Effects of ternary lipid compositions on optically trapping CTxB-microspheres in planar supported bilayers

To increase the complexity of our model system, we initially used lipid compositions that have had their ternary phase diagrams mapped out (e.g., *100, 101, 102*) (for example, dioleoylphosphatidylcholine (DOPC), SM, cholesterol) so that we know where our composition lies in the phase diagram—this will help us predict the expected biophysical properties (e.g., lateral and rotational diffusion, and ordering). We will employ fluors such as perylene and NBD-DPPE (NBD fluor-conjugated to dipalmitoyl-phosphatidylethanolamine) that preferentially partition into the liquid-ordered phase (*104-106*), and rhodamine-DPPE that preferentially partitions into the liquid-disordered phase (*101, 104, 105*), but have used, NBD-PC, NBD-DPPE and $DiIC_{18}$ lipid analogs to date.

In our preliminary results, we used fluorescence imaging to assess the domain formation and monitor our ability to manipulate bound CTxB-microspheres. Model membranes containing complex mixtures of POPC:SM:cholesterol (47:23:30 mol%) with 0.25 mol% NBD-DPPE lipid analog with our previously determined 0.05 mol% GM1 composition were used (Fig. 4.3). This composition has been shown previously in giant unilamellar vesicle studies that L_d and L_o states exist, and was therefore chosen as a starting point to assess whether CTxB-microsphere mobility was possible under our current optical calibration (*28*). Figure 4.3 shows a representation fluorescence image of phase separation occuring under these conditions, where CTxB-microspheres are visible at the edge of this separation (Fig 4.3 arrow). NBD-DPPE partions preferentially into the

L_o phase. CTxB-microspheres bound to GM1 were visible only in regions of NBD-DPPE. This is characteristic of GM1 to partition preferentially into regions of L_o making it an excellent domain marker. The mechanical manipulation of CTxB-microsphere was not possible under our current optical conditions. Reasons for the lack of trapping include a loss of infrared laser power through dichroic mirror and objective, therefore reducing our ability to manipulate the system with the incorporation of cholesterol, known to influence lateral diffusion properties. This is evident due to the substantial loss in efficiency at the dichroic mirror. $DiIC_{18}$ was used at 0.5 mol % under the same lipid composition. Preferential separation was not distinguishable with the incorporation of $DiIC_{18}$ (Fig. 4.4). Interestingly, uniformly bound CTxB-microspheres are visible under these conditions. Again, CTxB-microsphere mechanical manipulation was not possible.

Optical trapping is a functional tool to address underlying mechanisms in membrane structure and organization

Based on these preliminary results, we have demonstrated that optically trapping CTxB-microspheres is functional and, in principle, should pose no major problem in using it to answer key questions about membrane nucleation after optimization of our laser power at the sample plane. To avoid possible issues with co-aligning the trapping volume with the excitation volume (e.g., for FCS), we may combine total internal reflection excitation (which generates an evanescent field that extends ~100 nm into solution) with FCS and optical trapping (*48*).

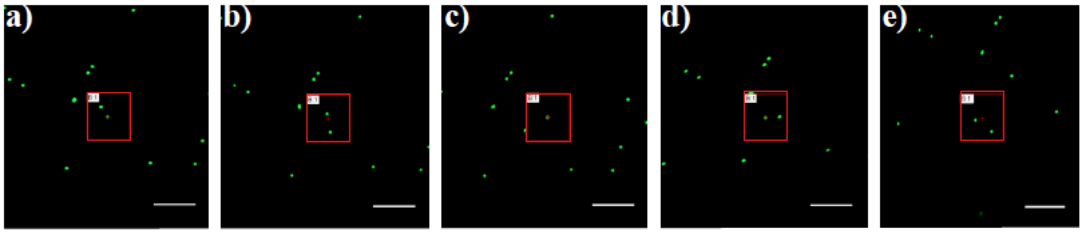

Figure 4.2 Time-lapsed (2, 4, 6, 8, 10 s) series depicting movement of LEP stage while trapping CTxB-microsphere binding GM1 (0.05 mol%) in POPC bilayer. CTxB-microsphere remains in plane upon release of optical trap showing that it retains its association with GM1 post mechanical manipulation. Cross-hair represents trapping potential well. Scale bar, 20 μm.

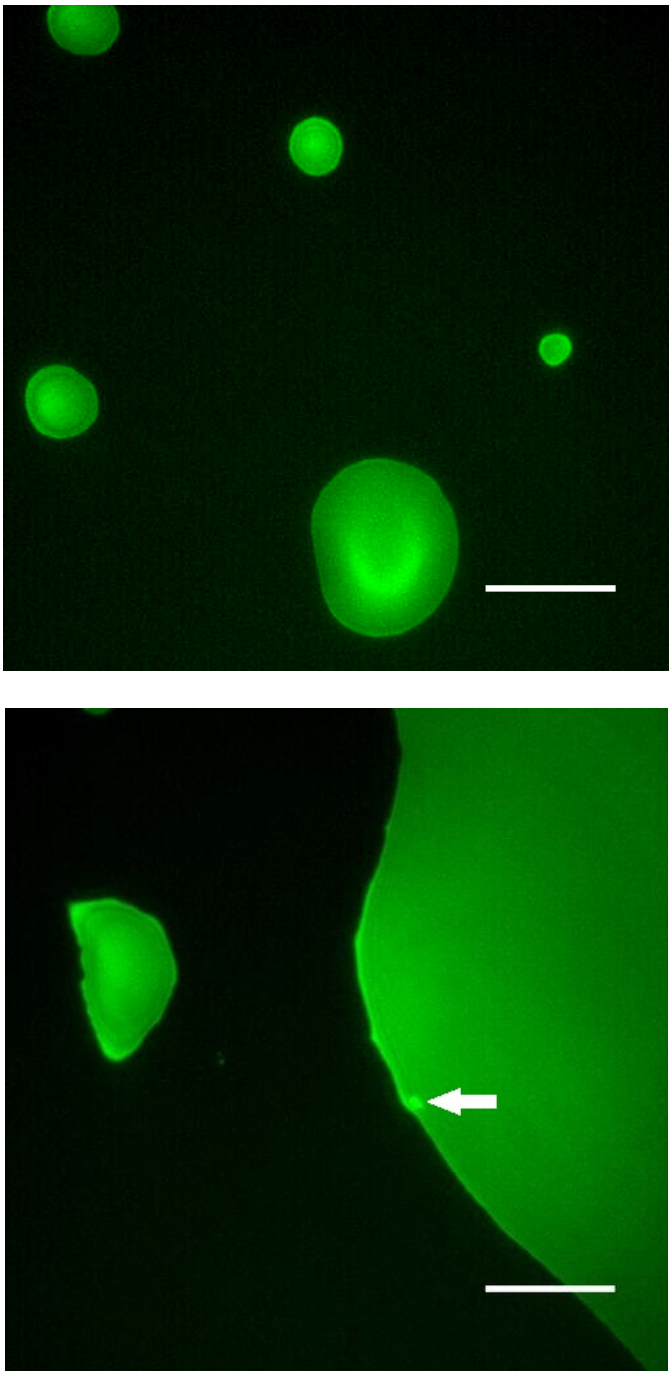

Figure 4.3 Fluorescence images of model membranes containing complex lipid compositions. Lipid bilayers contain POPC:SM:cholesterol (47:23:30 mol%) composition with 0.25 mol% NBD-DPPE lipid analog and 0.05 mol% GM1. NBD-DPPE and GM1 partition preferentially into L_o regions (green). Arrow depicts location of two CTxB-microspheres. Scale bar, 20 μm.

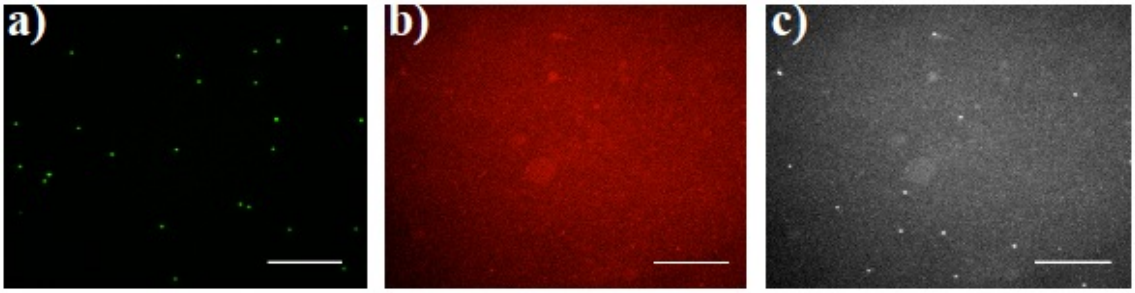

Figure 4.4 Fluorescence images of model membranes containing complex lipid compositions with $DiIC_{18}$ lipid analog. a) Depicts regions of covalently coupled CTxB-microsphere, b) fluorescently labeled $DiIC_{18}$ lipid analog distribution at low order preference, c) grayscale image of CTxB-microsphere location and lipid analog. Lipid bilayers contain POPC:SM:cholesterol [47:23:30 mol%] composition with 0.5 mol% $DiIC_{18}$ lipid analog and 0.05 mol% GM1. Scale bar, 20 μm.

V: Conclusion and future direction

Biomembranes are dynamic two-dimensional fluids that play a vital role in the functional of the cell. Their underlying organization and structure are poorly understood due to the transient nature and biocomplexity of living cells. Therefore, tools are needed to probe the dynamics of domain nucleation, what has been hypothesized to play an integral role in cellular function. To fill this gap in understanding, we have implemented an approach using a multimodal optical system to nucleate proto-domains associated with GM1 bound CTxB-microspheres (domain markers) in ternary biomimetic membranes, where we can control the complexity of our model system. Our ultimate goal is to answer fundamental questions about membrane structure and dynamics by non-invasively crosslinking cholesterol-rich domains using light as our crosslinker. This method of crosslinking will allow us to mechanically manipulate our system in real-time. We have currently implemented the use of FCS to study subsequent dynamics in our optical trapping system. By measuring changes in the biophysical properties (e.g., lateral and rotational diffusion, membrane order, oligomerization) of the lipids inside and outside of the nucleated domains, we will be able to determine whether crosslinking is sufficient to drive domain formation.

To date, we have incorporated an optical system with a single beam optical trap with the ability to mechanically manipulate the lateral location of CTxB-microspheres in GM1 (0.05 mol%) containing POPC bilayers supporting the proof of concept of our multimodal system containing the ability to assess lateral mobility of lipid analogs (0.1 mol% NBD-PC) with FCS under the same conditions. The conserved binding between

CTxB-microspheres and GM1 after trapping supports our binding specificity experiments of covalently coupling CTxB to fluorescent microspheres. The optimization of GM1 incorporation at various concentrations was assessed to determine and enhance our model system. GM1 does affect the lateral diffusion of lipid analog NBD-PC incorporation. These studies were done to determine potential concentrations of GM1 necessary to mechanically manipulate CTxB-microspheres.

A transition to complex bilayers containing multiple lipid species demonstrated further optimization of our trapping power (10 pN through the objective from the laser source) is still needed. In addition to optimizing our ability to trap within complex bilayers, a future approach to incorporate the use of a Langmuir trough to produce asymmetrical bilayers should be explored. The trough will also better mimic GM1's physiological incorporation to the outer leaflet of the plasma membrane. As the optimization of our trapping system moves forward, decreasing microsphere size will be explored to reduce the effects of size implications on our membrane. Finally, the effects of optical trapping on live cells will be our ultimate experimental goal to answer fundamental questions about membrane organization and structure that leads to biological function.

Importantly these results will allow us to modify our understanding of these systems and develop new models about their roles in the plasma membrane and signal transduction. In future experiments, we will further extend this to inducing domain nucleation via HOT in RBL mast cells, using light as the crosslinker instead of antigen. To monitor the success, we will assess tyrosine phosphorylation, calcium mobilization

and degranulation on the single cell level. Because our imaging system is multimodal, we can easily monitor these various activities simultaneously while manipulating molecules with the HOT (*48*). While colloidal gold is not fluorescent, it may prove to be a better handle for optical trapping and used in conjunction with fluorescent probes that partition with specificity within the bilayer (*106*).

References

(1) Singer, S.J., and Nicolson, G.L. (1972) The fluid mosaic model of the structure of cell membranes. *Science*. **175**, 720-731

(2) Goertz, M.P., and Stottrup, B.L. (2011) Mechanical properties of phospholipid-based biolubricant films and membranes. in *Surfactants in Tribology* ed.), pp. 119-142, Taylor and Francis Group, LLC

(3) Buehler, L.K. (2016) *Cell Membranes*: Garland Science

(4) Nicolson, G.L. (2013) The fluid-mosaic model of membrane structure: still relevant to understanding the structure, function and dynamics of biological membranes after more than 40 years. *Biochim. Biophys. Acta*. **1838**, 1451-1466

(5) Sheets, E.D., Chen, L., and Thompson, N.L. (1997) Decreased IgG-FcεRII dissociation kinetics in the presence of a protein antigen. *Mol. Immunol.* **34**, 519-526

(6) Sheets, E.D., Simson, R., and Jacobson, K. (1995) New insights into membrane dynamics from the analysis of cell surface interactions by physical methods. *Curr. Opin. Cell Biol.* **7**, 707-714

(7) Sheets, E.D., Holowka, D., and Baird, B. (1999) Membrane organization in immunoglobulin E receptor signaling. *Curr. Opin. Chem. Biol.* **3**, 95-99

(8) Siraganian, R.P. (2003) Mast cell signal transduction from the high-affinity IgE receptor. *Curr. Opin. Immunol.* **15**, 639-646

(9) Sheets, E.D., Holowka, D., and Baird, B. (1999) Critical role for cholesterol in Lyn-mediated tyrosine phosphorylation of FcεRI and their association with detergent-resistant membranes. *J. Cell Biol.* **145**, 877-887

(10) Holowka, D., Sheets, E.D., and Baird, B. (2000) Interactions between FcεRI and lipid raft components are regulated by the actin cytoskeleton. *J. Cell Sci.* **113**, 1009-1019

(11) Davey, A.M., Walvick, R.P., Liu, Y., Heikal, A.A., and Sheets, E.D. (2007) Membrane order and molecular dynamics associated with IgE receptor cross-linking in mast cells. *Biophys. J.* **92**, 343-355

(12) Razzaq, T.M., Ozegbe, P., Jury, E.C., Sembi, P., Blackwell, N.M., and Kabouridis, P.S. (2004) Regulation of T-cell receptor signalling by membrane microdomains. *Immunology*. **113**, 413-426

(13) Cheng, P.C., Cherukuri, A., Dykstra, M., Malapati, S., Sproul, T., Chen, M.R., and Pierce, S.K. (2001) Floating the raft hypothesis: the roles of lipid rafts in B cell antigen receptor function. *Semin. Immunol.* **13**, 107-114

(14) Lajoie, P., Goetz, J.G., Dennis, J.W., and Nabi, I.R. (2009) Lattices, rafts, and scaffolds: domain regulation of receptor signaling at the plasma membrane. *J. Cell Biol.* **185**, 381-385

(15) Horejsi, V., and Hrdinka, M. (2014) Membrane microdomains in immunoreceptor signaling. *FEBS Lett.* **588**, 2392-2397

(16) Linder, R., and Naim, H.Y. (2009) Domains in biological membranes. *Exp. Cell Res.* **315**, 2871-2878

(17) Pike, L.J. (2005) Growth factor receptors, lipid rafts and caveolae: an evolving story. *Biochim. Biophys. Acta*. **1746**, 260-273
(18) Simons, K., and Toomre, D. (2000) Lipid rafts and signal transduction. *Mol. Cell. Biol.* **1**, 31-41
(19) Almeida, P.F.F. (2009) Thermodynamics of lipid interactions in complex bilayers. *Biochim. Biophys. Acta*. **1788**, 72-85
(20) Almeida, P.F.F., Pokorny, A., and Hinderliter, A. (2005) Thermodynamics of membrane domains. *Biochim. Biophys. Acta*. **1720**, 1-13
(21) Ahmed, H.A. (1993) Measurement of cholesterol in membranes. in *Methods Mol. Biol.* (Graham, J.M., and Higgins, J.A., ed.), Totowa, NJ, Humana Press
(22) Anderson, T.G., and McConnell, H.M. (2002) A thermodynamic model for extended complexes of cholesterol and phospholipid. *Biophys. J.* **83**, 2039-2052
(23) Jacobson, K., Sheets, E.D., and Simson, R. (1995) Revisiting the fluid mosaic model of membranes. *Science*. **268**, 1441-1442
(24) Gennis, R.B. (1989) *Biomembranes: Molecular Structure and Function*, New York: Springer
(25) Almeida, P.F., Vaz, W.L.C., and Thompson, T.E. (1993) Percolation and diffusion in three-component lipid bilayers: effect of cholesterol on an equimolar mixture of two phophatidylcholines. *Biophys. J.* **64**, 399-412
(26) London, E. (2002) Insights into lipid raft structure and formation from experiments in model membranes. *Curr. Opin. Struct. Biol.* **12**, 480-486
(27) Mukherjee, S., Ghosh, R.N., and Maxfield, F.R. (1997) Endocytosis. *Physiol. Rev.* **77**, 759-803
(28) Veatch, S.L., and Keller, S.L. (2005) Miscibility phase diagrams of giant vesicles containing sphingomyelin. *Phys. Rev. Lett.* **94**, 148101
(29) Ariola, F.S., Li, Z., Cornejo, C., Bittman, R., and Heikal, A.A. (2009) Membrane fluidity and lipid order in ternary giant unilamellar vesicles using a new bodipy-cholesterol derivative. *Biophys. J.* **96**, 2696-2708
(30) Almeida, P.F.F., Sohma, H., Rasch, K.A., Wieser, C.M., and Hinderliter, A. (2005) Allosterism in membrane binding: a common motif of the annexins? *Biochemistry*. **44**, 10905-10913
(31) Fealey, M.E., Gauer, J.W., Kempka, S.C., Miller, K., Nayak, K., Sutton, R.B., and Hinderliter, A. (2012) Negative coupling as a mechanism for signal propagation between C2 domains of synaptotagmin I. *PLoS ONE*. **7**, e467748
(32) Gauer, J.W., Knutson, K.J., Jaworski, S.R., Rice, A.M., Rannikko, A.M., Lentz, B.R., and Hinderliter, A. (2013) Membrane modulates affinity for calcium ion to create an apparent cooperative binding response by annexin a5. *Biophys. J.* **104**, 2437-2447
(33) Hinderliter, A., Almeida, P.F.F., Creutz, C.E., and Biltonen, R.L. (2001) Domain formation in a fluid mixed lipid bilayer modulated through binding of the C2 protein motif. *Biochemistry*. **40**, 4181-4191
(34) Burns, A.R., Frankel, D.J., and Buranda, T. (2005) Local mobility in lipid domains of supported bilayers characterized by atomic force microscopy and fluorescence correlation spectroscopy. *Biophys. J. BioFAST*. **in press**,

(35) Hoh, J.H., and Hansma, P.K. (1992) Atomic force microscopy for high-resolution imaging in cell biology. *Trends Cell Biol.* **2**, 208-213
(36) Braun, J., Abney, J.R., and Owicki, J.C. (1987) Lateral interactions among membrane proteins. Valid estimates based on freeze-fracture electron microscopy. *Biophys. J.* **52**, 427-439
(37) Shotton, D. (1993) An introduction to digital image processing and image display in electronic light microscopy. in *Electronic Light Microscopy: Techniques in Modern Biomedical Microscopy* (Shotton, D., ed.), pp. 39-70, New York, Wiley-Liss
(38) Howland, M.C., Szmodis, A.W., Sanii, B., and Parikh, A.N. (2007) Characterization of physical properties of supported phospholipid membranes using imaging ellipsometry at optical wavelengths. *Biophys. J.* **92**, 1306-1317
(39) Sackmann, E. (1996) Supported membranes: scientific and practical applications. *Science*. **271**, 43-48
(40) Abney, J.R., Scalettar, B.A., and Thompson, N.L. (1992) Evanescent interference patterns for fluorescence microscopy. *Biophys. J.* **61**, 542-552
(41) Almeida, P.F.F., Vaz, W.L.C., and Thompson, T.E. (1992) Lateral diffusion and percolation in two-phase, two-component lipid bilayers. Topology of the solid-phase domains in-plane and across the lipid bilayer. *Biochemistry*. **31**, 7198-7210
(42) Almeida, P.F.F., Vaz, W.L.C., and Thompson, T.E. (1992) Lateral diffusion in the liquid phases of dimyristoylphosphatidylcholine/cholesterol lipid bilayers: a free volume analysis. *Biochemistry*. **31**, 6739-6747
(43) Almeida, P.F.F., Vaz, W.L.C., and Thompson, T.E. (2005) Lipid diffusion, free area, and molecular dynamics simulations. *Biophys. J. BioFAST*. **in press**.
(44) Thompson, N.L. (1991) Fluorescence correlation spectroscopy. in *Topics in Fluorescence Spectroscopy, Volume 1: Techniques* (Lakowicz, J.R., ed.), pp. 337-378, New York, Plenum Press
(45) Thompson, N.L., Lieto, A.M., and Allen, N.W. (2002) Recent advances in fluorescence correlation spectroscopy. *Curr. Opin. Struct. Biol.* **12**, 634-641
(46) Tamm, L.K., and McConnell, H.M. (1985) Supported phospholipid bilayers. *Biophys. J.* **47**, 105-113
(47) Tamm, L.K., and Tatulian, S.A. (1993) Orientation of functional and nonfunctional PTS permease signal sequences in lipid bilayers. A polarized attenuated total reflection infrared study. *Biochemistry*. **32**, 7720-7726
(48) Kyoung, M., Karunwi, K., and Sheets, E.D. (2007) A versatile multi-mode microscope to probe and manipulate nanoparticles and biomolecules. *J. Microsc.* **225**, 137-146
(49) Kyoung, M., and Sheets, E.D. (2008) Vesicle diffusion close to a membrane: intermembrane interactions measured with fluorescence correlation spectroscopy. *Biophys. J.* **95**, 5789-5797
(50) Vats, K., Knutson, K., Hinderliter, A., and Sheets, E.D. (2010) Peripheral protein organization and its influence on lipid diffusion in biomimetic membranes. *ACS Chem. Biol.* **5**, 393-403

(51) Kalb, E., Frey, S., and Tamm, L.K. (1992) Formation of supported planar bilayers by fusion of vesicles to supported phospholipid monolayers. *Biochim. Biophys. Acta*. **1103**, 307-316
(52) Cheng, Y., Boden, N., Bushby, R., Clarkson, S., Evans, S.D., Knowles, P.F., Marsh, A., and Miles, R. (1998) Attenuated total reflection fourier transform infrared spectroscopic characterization of fluid lipid bilayers tethered to solid supports. *Langmuir*. **14**, 839-834
(53) Kim, J., Kim, G., and Cremer, P.S. (2001) Investigations of water structure at the solid/liquid interface in the presence of supported lipid bilayers by vibrational sum frequency spectroscopy. *Langmuir*. **17**, 7255-7260
(54) von Tscharner, V., and McConnell, H.M. (1981) An alternative view of phospholipid phase beahvior at the air-water interface. *Biophys. J.* **36**, 409-419
(55) Miller, L.W., (2008) *Probes and tags to study biomolcular function: for proteins, RNA, and membranes*: Wiley-VCH
(56) Staros, J.V., Wright, R.W., and Swingle, D.M. (1986) Enhancement by N-hydroxysulfosuccinimide of water-soluble carbodiimide-mediated coupling reactions. *Anal. Biochem.* **156**, 220-222
(57) Hermanson, G.T. (1996) *Bioconjugate Techniques*, San Diego: Academic Press
(58) Madge, D.E., Elson, E.L., and Webb, W.W. (1972) Thermodynamics fluctuations in the reacting system: measurement by fluorescence correlation spectroscopy. *Biopolymers*. **13**, 29-61
(59) Schwille, P., Bieschke, J., and Oehlenschläger, F. (1997) Kinetic investigations by fluorescence correlation spectroscopy: the analytical and diagnostic potential of diffusion studies. *Biophys. Chem.* **66**, 211-228
(60) Schwille, P., Haupts, U., Maiti, S., and Webb, W.W. (1999) Molecular dynamics in living cells observed by fluorescence correlation spectroscopy with one- and two-photon excitation. *Biophys. J.* **77**, 2251-2265
(61) Schwille, P., Korlach, J., and Webb, W.W. (1999) Fluorescence correlation spectroscopy with single-molecule sensitivity on cell and model membranes. *Cytometry*. **36**, 176-182
(62) Schwille, P., Kummer, S., Heikal, A.A., Moerner, W.E., and Webb, W.W. (2000) Fluorescence correlation spectroscopy reveals fast optical excitation-driven intramolecular dynamics of yellow fluorescent proteins. *Proc Natl Acad Sci U S A*. **97**, 151-156
(63) Schwille, P., Meyer-Almes, F.-J., and Rigler, R. (1997) Dual-color fluorescence cross-correlation spectroscopy for multicomponent diffusional analysis in solution. *Biophys. J.* **72**, 1878-1886
(64) Schwille, P., and Haustein, E. Fluorescence correlation spectroscopyed.
(65) Rigler, R., Mets, U., Widengren, S., and Kask, P. (1993) Fluorescence correlation spectroscopy with high countrate and low backgroup: analysis of translational diffusion. *Eur. Biophys. J.* **22**, 169-175
(66) Korlach, J., Schwille, P., Webb, W.W., and Feigenson, G.W. (1999) Characterization of lipid bilayer phases by confocal microscopy and fluorescence correlation spectroscopy. *Proc. Natl. Acad. Sci. USA*. **96**, 8461-8466

(67) Bialek, W., and Setayeshgar, S. (2005) Physical limits to biochemical signaling. *Proc. Natl. Acad. Sci. USA*. **102**, 10040-10045
(68) Nyquist, H. (1928) Thermal agitation of electric charge in conductors. *Phys. Rev. Lett.* **32**, 110-113
(69) Callen, H.B., and Welton, T.A. (1951) Irreversibility and generalized noise. *Phys. Rev. Lett.* **83**, 34
(70) Ruttinger, S., Buschmann, V., Kramer, B., Erdmann, R., Macdonald, R., and Koberling, F. (2008) Comparison and accuracy of methods to determine the confocal volume for quantitative fluorescence correlation spectroscopy. *J. Microsc.* **232**, 343-352
(71) Hess, S.T., Huang, S., Heikal, A.A., and Webb, W.W. (2002) Biological and chemical applications of fluorescence correlation spectroscopy: a review. *Biochemistry*. **41**, 697-705
(72) Kim, S.A., and Schwille, P. (2003) Intracellular applications of fluorescence correlation spectroscopy: prospects for neuroscience. *Curr. Opin. Neurobiol.* **13**, 583-590
(73) Sheets, E.D. (1997) Detecting transient confinement in the plasma membrane with single particle trackinged, *Chemistry* Chapel Hill, NC: University of North Carolina at Chapel Hill. pp. 88.
(74) Ashkin, A. (1997) Optical trapping and manipulation of neutral particles using lasers. *Proc. Natl. Acad. Sci. USA*. **94**, 4853-4860
(75) Ashkin, A., Dziedzic, J.M., Bjorkholm, J.E., and Chu, S. (1986) Observation of a single-beam gradient force optical trap for dielectric particles. *Opt. Lett.* **11**, 288-290
(76) Gabor, D. (1948) A new microscopic principles. *Nature*. **161**, 777-778
(77) Gabor, D. (1949) Microscopy by reconstructed wavefronts: II. *Proc. Roy. Soc.* **197**, 454-487
(78) Ashkin, A. (1970) Acceleration and trapping of particles by radiation pressure. *Phys. Rev. Lett.* **24**, 156
(79) Sonnino, S., Mauri, L., Chigorno, V., and Prinetti, A. (2006) Gangliosides as components of lipid membrane domains. *Glycobiol.* **17**, 1R-13R
(80) Weng, K.C., Kanter, J.L., Robinson, W.H., and Frank, C.W. (2006) Fluid supported lipid bilayers containing monosialogangliosdie GM1: a QCM-D and FRAP study. *Biointerphases*. **50**, 76-84
(81) Goins, B., Masserini, M., Barisas, B.G., and Freire, E. (1986) Lateral diffusion of ganglioside GM1 in phospholipid bilayer membranes. *Biophys. J.* **49**, 849-856
(82) Love, S., Louis, D., and Ellison, D.W. (2008) *Greenfield's Neuropathology*: CRC Press
(83) Maglione, V., Marchi, P., Di Pardo, A., Lingrell, S., Horkey, M., Tidmarsh, E., and Sipione, S. (2010) Impaired ganglioside metabolism in Huntington's disease and neuroprotective role of GM1. *J. Neurosci.* **30**, 4072-4080
(84) Becucci, L., Vizza, F., Duarte, Y., and Guidelli, R. (2014) The GM1 ganglioside forms GM1-rich gel phase microdomains within lipid rafts. *Coatings*. **4**, 450-464

(85) Rog, T., and Vattulainen, I. (2014) Cholesterol, sphingolipids, and glycolipids: what do we know about their role in raft-like membranes. *Chem. Phys. Lipids*. **184**, 82-104
(86) Atta, D., and Okasha, A. (2015) Single molecule laser spectroscopy. *Spectrochim. Acta A: Molec. Biomolec. Spectrosc.* **135**, 1173-1179
(87) Singh, A.P., and Wohland, T. (2014) Applications of imaging fluorescence correlation spectroscopy. *Curr. Opin. Chem. Biol.* **20**, 29-35
(88) Klymchenko, A., and Kreder, R. (2014) Fluorescent probes for lipid rafts: from model membranes to living cells. *Chem. Biol.* . **21**,
(89) Sheets, E.D., Lee, G.M., Simson, R., and Jacobson, K. (1997) Transient confinement of a glycosylphosphatidylinositol-anchored protein in the plasma membrane. *Biochemistry*. **36**, 12449-12458
(90) Lee, G.M., and Jacobson, K. (1994) Lateral mobility of lipids in membranes. *Curr. Top. Membranes*. **40**, 111-142
(91) Kelly, C.V., Wakefield, D.L., Holowka, D., Craighead, H.G., and Baird, B.A. (2014) Near-field fluorescence cross-correlation spectroscopy on planar membranes. *ACS Nano*. **8**, 7392-7404
(92) Wang, R., Shi, J., Shreve, A.P., Chen, L., and Swanson, B.I. (2004) Evidence of cholera aggregation on GM1-decorated lipid bilayers. *Colloids Surf., B*. **33**, 45-51
(93) Hammond, A.T., Heberle, F.A., Baumgart, T., Holowka, D., Baird, B., and Feigenson, G.W. (2005) Crosslinking a lipid raft component triggers liquid ordered-liquid disordered phase separation in model plasma membranes. *Proc. Natl. Acad. Sci. USA*. **102**, 6320-6325
(94) Anderson, R.G., and Jacobson, K. (2002) A role for lipid shells in targeting proteins to caveolae, rafts, and other lipid domains. *Science*. **296**, 1821-1825
(95) Gross, S.P. (2003) Application of optical traps *in vivo*. *Methods Enzymol.* **361**, 162-174
(96) Curtis, J.E., Koss, B.A., and Grier, D.G. (2002) Dynamic holographic optical tweezers. *Optics Comm.* **207**, 169-175
(97) Melville, H., Milne, G.F., Spalding, G.C., Sibbett, W., Dholakia, K., and McGloin, D. (2003) Optical trapping of three-dimensional structures using dynamic holograms. *Optics Expr.* **11**, 3562-3567
(98) Yamamoto, J., and Iwai, T. (2012) Highly controllable optical tweezers. *Curr. Pharm. Biotechnol.* **13**, 2655-2662
(99) Kirkham, G.R., Britchford, E., Upton, T., Ware, J., Gibson, G.M., Devaud, Y., Ehrbar, M., Padgett, M., Allen, S., Buttery, L.D., and Shakesheff, K. (2015) Precision assembly of complex cellular microenvironments using holographic optical tweezers. *Sci. Rep.* **5**, 8577
(100) Feigenson, G.W., and Buboltz, J.T. (2001) Ternary phase diagram of dipalmitoyl-PC/dilauroyl-PC/cholesterol: nanoscopic domain formation driven by cholesterol. *Biophys. J.* **80**, 2775-2788
(101) Baumgart, T., Hess, S.T., and Webb, W.W. (2003) Imaging coexisting fluid domains in biomembrane models coupling curvature and line tension. *Nature*. **425**, 821-824

(102) Veatch, S.L., and Keller, S.L. (2003) Separation of liquid phases in giant vesicles of ternary mixtures of phospholipids and cholesterol. *Biophys. J.* **85**, 3074-3083
(103) Dufresne, E.R. (1999) Hydrodynamic Coupling and Optical Patterning of Many-particle Colloidal Systemsed^eds, *Physics* Chicago, IL: Univesity of Chicago.
(104) Hunt, G., Baumgart, T., and Feigenson, G.W. (2002) Partitioning of fluorescent probes between coexisting bilayers phases. *Biophys. J.* **84**, 187a
(105) Dietrich, C., Bagatolli, L.A., Volovyk, Z.N., Thompson, N.L., Levi, M., Jacobson, K., and Gratton, E. (2001) Lipid rafts reconstituted in model membranes. *Biophys. J.* **80**, 1417-1428
(106) Sezgin, E., Levental, I., Grzybek, M., Schwartzmann, G., Mueller, V., Honigmann, A., Belov, V.N., Eggeling, C., Coskun, Ü., Simons, K., and Schwille, P. (2012) Partioning, diffusion, and ligand binding of raft lipid analogs in model and cellular plasma membranes. *Biochim. Biophys. Acta*. **1818**, 1777-1784

Appendix A

Holographic optical trapping

Sample preparation

1. Apply ~1 inch long strip of double sticky tape to each of the long sides of a slide glass. The strips of tape should be fairly thin to allow space between the strips for the sample solution later.

2. Dilute silica microspheres, 0.8 μm in diameter (SS03N, Bangs Laboratories, Inc.) ~100× with water and add about 50 μL to the space between the sandwich and seal with nail polish. (FluoSpheres are in the refrigerator in 37ºC.)

Turn on IR laser

1. Turn on power strip
2. Turn the key on laser control box
3. Press flashing "enable" button on control box
4. Adjust power by pressing button twice
5. Laser percent value will turn red to adjust knob to desired power
6. Exit by pressing button twice
7. Turn on wide field light (tungsten lamp)
8. Turn on LEP controller
9. Turn on power of shutters' controller for IR laser
10. Turn on CCD

11. Open IR shutter

Turn on SLM

1. Plug in power cord to SLM control box before turning on the computer
2. Turn on computer
3. Open PCIe LabVIEW software
4. Open the interface.ini in LabVIEW and run program

Project image on SLM

1. Turn off “SLM Power”
2. Choose desired image
3. Turn on “SLM Power”

Optical trapping

1. Use oil immersion 1.4 NA objective and wide field light for bead visualization
2. Use shutter controls to block laser and release trap
3. Use LEP controller to move stage relative to sample

Appendix B

Fluorescence correlation spectroscopy

Note: The PMTs are very sensitive to detectors to light. High power lasers and highly concentrated samples can damage them. Room light should not be on while the detector is on to avoid damage.

Turn on laser

1. Turn on Cobolt Calypso 491 nm laser
2. Turn on LEP controller and the computer
3. Turn on the power of the shutters' controller for the UV-Vis box
4. Open Flex02 program
5. Use the oil immersion 1.4 NA objective or water immersion 1.2 NA objective
6. Turn turret beneath filter cute to desired wavelength
7. Be sure to remove Wollaston prism underneath objective and analyzer from emission path. Close shutter to eyepiece. Close epi field diaphragm.
8. Change path of port selection to right (towards PMTs)

Prepare control sample

9. Place water or oil (depending on objective chosen) on objective
10. Carefully place 22 mm × 22 mm glass coverslip on oil
11. Pipet ~70 μL of 2 nM rhodamine green on center of coverslip
12. Turn on PMT A and PMT B (check that fans are working)

13. Monitor dark counts (should be less than 0.02 kHz photon counts)
14. Open shutter (n.c. to n.o.)
15. You will now see a spike in detection
16. Increase ND filters if detection is >700 kHz
17. The optical fiber is adjusted in x, y, and z direction for both PMTs to obtain maximum photon counts
18. Set parameters according to acquisition specifications

Turn off system

1. Close laser shutter
2. Turn off PMTs
3. Turn off electronics (LEP controller, laser shutter, computer)
4. Turn off laser